

AFWAL-TR-83-3050

CORRELATION OF EXPERIMENTAL AND QUASI-3D THEORETICAL
AIRLOADS ON THE OSCILLATING LANN SUPERCRITICAL WING
MODEL

A. Steinginga
R. Houwink

National Aerospace Laboratory (NLR)
Amsterdam, Netherlands



May 1983

Final Report for Period April 1982 - December 1982

Approved for public release; distribution unlimited.

FLIGHT DYNAMICS LABORATORY
AIR FORCE WRIGHT AERONAUTICAL LABORATORIES
AIR FORCE SYSTEMS COMMAND
WRIGHT-PATTERSON AIR FORCE BASE, OHIO 45433

20070919105

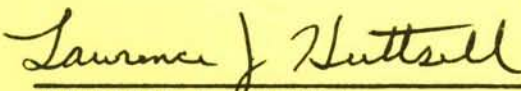
Best Available Copy

NOTICE

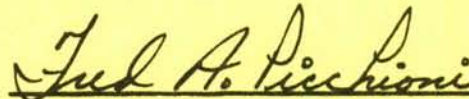
When Government drawings, specifications, or other data are used for any purpose other than in connection with a definitely related Government procurement operation, the United States Government thereby incurs no responsibility nor any obligation whatsoever; and the fact that the government may have formulated, furnished, or in any way supplied the said drawings, specifications, or other data, is not to be regarded by implication or otherwise as in any manner licensing the holder or any other person or corporation, or conveying any rights or permission to manufacture use, or sell any patented invention that may in any way be related thereto.

This report has been reviewed by the Office of Public Affairs (ASD/PA) and is releasable to the National Technical Information Service (NTIS). At NTIS, it will be available to the general public, including foreign nations.

This technical report has been reviewed and is approved for publication.

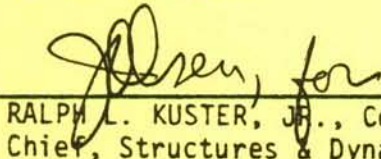


LAWRENCE J. HUTTSELL
Aerospace Engineer
Aeroelastic Group



FREDERICK A. PICCHIONI, Lt Col, USAF
Chief, Analysis & Optimization Branch
Structures & Dynamics Division

FOR THE COMMANDER



RALPH L. KUSTER, JR., Colonel, USAF
Chief, Structures & Dynamics Division

"If your address has changed, if you wish to be removed from our mailing list, or if the addressee is no longer employed by your organization please notify AFWAL/FIBRE W-PAFB, OH 45433 to help us maintain a current mailing list".

Copies of this report should not be returned unless return is required by security considerations, contractual obligations, or notice on a specific document.

UNCLASSIFIED

SECURITY CLASSIFICATION OF THIS PAGE (When Data Entered)

REPORT DOCUMENTATION PAGE		READ INSTRUCTIONS BEFORE COMPLETING FORM
1. REPORT NUMBER AFWAL-TR-83-3050	2. GOVT ACCESSION NO.	3. RECIPIENT'S CATALOG NUMBER
4. TITLE (and Subtitle) CORRELATION OF EXPERIMENTAL AND QUASI-3D THEORETICAL AIRLOADS ON THE OSCILLATING LANN SUPERCRITICAL WING MODEL		5. TYPE OF REPORT & PERIOD COVERED Final Technical Report Apr 1982 - Dec 1982
		6. PERFORMING ORG. REPORT NUMBER NLR TR 83003 U
7. AUTHOR(s) A. Steinginga H. Houwink		8. CONTRACT OR GRANT NUMBER(s) F33615-79-C-3030
9. PERFORMING ORGANIZATION NAME AND ADDRESS National Aerospace Laboratory (NLR) Amsterdam, the Netherlands		10. PROGRAM ELEMENT, PROJECT, TASK AREA & WORK UNIT NUMBERS PE 62201F Project/Task/WU 2401/02/36
11. CONTROLLING OFFICE NAME AND ADDRESS Structures and Dynamics Division (FIB) Air Force Wright Aeronautical Laboratory Wright-Patterson AFB OH 45433		12. REPORT DATE May 1983
		13. NUMBER OF PAGES 63
14. MONITORING AGENCY NAME & ADDRESS (if different from Controlling Office)		15. SECURITY CLASS. (of this report) Unclassified
		15a. DECLASSIFICATION/DOWNGRADING SCHEDULE
16. DISTRIBUTION STATEMENT (of this Report) Approved for public release; distribution unlimited		
17. DISTRIBUTION STATEMENT (of the abstract entered in Block 20, if different from Report)		
18. SUPPLEMENTARY NOTES		
19. KEY WORDS (Continue on reverse side if necessary and identify by block number) Pressure Measurements Correlation Supercritical Wing Quasi-3D Transonic Flow Theoretical Airloads Unsteady Aerodynamics Wind-Tunnel Tests		
20. ABSTRACT (Continue on reverse side if necessary and identify by block number) Correlation of theoretical and experimental unsteady airloads on an oscillating semi-span model of a transport-type supercritical wing (LANN Model) was conducted. The theoretical method is a quasi-3D method which combines 2D transonic small perturbation theory (LTRAN-NLR code) with 2D and 3D subsonic theory (Doublet-Lattice method). Parameters in this correlation are Mach number, frequency, mean angle of attack, and oscillation amplitude.		

FOREWORD

AFOSR Grant 80-0136, "Transonic Wind Tunnel Measurements on a Supercritical Wing" was initiated by the Structures and Dynamics Division (FIB) of the Air Force Wright Aeronautical Laboratories (AFWAL). The objective of this effort was to obtain experimental data on a supercritical wing to guide improvements in transonic unsteady aerodynamics. This effort was a part of a cooperative program involving Lockheed-Georgia Air Force, NASA, and NLR. This cooperative effort has become known as the LANN program.

Under contract F33615-79-C-3030, NLR conducted aerodynamic analyses and correlated with the available test data. The principal investigators on the grant at NLR were J. J. Horsten, R. G. den Boer, and R. J. Zwaan. The principal investigators on the contract were A. Steinginga, R. Houwink, and R. J. Zwaan. The AFWAL project engineer was L. J. Huttshell and the work unit was 24010236.

This report presents the correlation of theoretical and experimental unsteady airloads on the supercritical transport-type wing (LANN Model). Parameters in the correlation are Mach number, frequency, mean angle of attack, and oscillation amplitude.

TABLE OF CONTENTS

<u>SECTION</u>	<u>PAGE</u>
1 INTRODUCTION	1
2 EXPERIMENTAL DATA	1
3 THE COMPUTATIONAL METHOD	2
4 COMPUTATIONS FOR THE LANN MODEL	4
5 PRESENTATION AND DISCUSSION OF RESULTS	8
5.1 Steady Pressure Distribution	8
5.2 Unsteady Airloads as Function of Mach Number	8
5.2.1 Quasi-Steady Results	8
5.2.2 Unsteady Results for $f = 24$ Hz	11
5.2.3 Unsteady Results for $f = 48$ Hz	13
5.3 Unsteady Airloads as Function of Frequency	13
5.4 Unsteady Airloads as Function of Mean Angle of Attack	14
6 CONCLUSIONS	15
APPENDIX: EXPERIMENTAL DATA FOR THE COMPUTATIONAL TEST CASES	16
REFERENCES	55

LIST OF ILLUSTRATIONS

<u>FIGURE</u>		<u>PAGE</u>
1	Schematic View of Test Set-up	31
2	Wing Planform and Measuring Points	31
3	Test Conditions for LANN Model	32
4	Influence of Mach Number and Frequency on Node Line Position . .	32
5	Outline of Quasi-3D Method	33
6	Mean Steady Pressure Distributions on Section 3	34
7	Quasi-Steady Pressure Distributions on Section 3 ($\alpha_0 = 0.6$ deg) .	35
8	Quasi-Steady Sectional Lift Coefficient ($\alpha_0 = 0.6$ deg)	36
9	Quasi-Steady Section Moment Coefficients ($\alpha_0 = 0.6$ deg)	37
10	Quasi-Steady Wing Lift and Moment Coefficients ($\alpha_m = 0.6$ deg) . .	38
11	Unsteady Pressure Distributions on Section 3 ($\alpha_0 = 0.6$ deg, f = 24 Hz)	39
12	Unsteady Sectional Lift Coefficients ($\alpha_0 = 0.6$ deg, f = 24 Hz) . .	40
13	Unsteady Sectional Moment Coefficients ($\alpha_0 = 0.6$ deg, f = 24 Hz) .	41
14	Unsteady Wing Lift and Moment Coefficients ($\alpha_m = 0.6$ deg, f = 24 Hz)	42
15	Unsteady Pressure Distributions on Section 3 ($\alpha_0 = 0.6$ deg, f = 48 Hz)	43
16	Unsteady Sectional Lift Coefficients ($\alpha_0 = 0.6$ deg, f = 48 Hz) . .	44
17	Unsteady Sectional Moment Coefficients ($\alpha_0 = 0.6$ deg, f = 48 Hz) .	45
18	Unsteady Wing Lift and Moment Coefficients ($\alpha_m = 0.6$ deg, f = 48 Hz)	46
19	Quasi-Steady and Unsteady Pressure Distributions on Section 3 ($\alpha_0 = 2.6$ deg, $M_\infty = 0.77$)	47
20	Unsteady Sectional Lift Coefficients ($\alpha_0 = 2.6$ deg, $M_\infty = 0.77$) . .	48

LIST OF ILLUSTRATIONS (Cont'd)

<u>FIGURE</u>		<u>PAGE</u>
21	Unsteady Sectional Moment Coefficient ($\alpha_0 = 2.6$ deg, $M_\infty = 0.77$) .	49
22	Unsteady Wing Lift and Moment Coefficients ($\alpha_m = 2.6$ deg, $M_\infty = 0.77$)	50
23	Unsteady Pressure Distributions on Section 3 ($M_\infty = 0.77$, $f = 24$ Hz)	51
24	Unsteady Sectional Lift Coefficients ($M_\infty = 0.77$, $f = 24$ Hz) . . .	52
25	Unsteady Sectional Moment Coefficients ($M_\infty = 0.77$, $f = 24$ Hz) . .	53
26	Unsteady Wing Lift and Moment Coefficients ($M_\infty = 0.77$, $f = 24$ Hz)	54

LIST OF TABLES

<u>TABLE</u>		<u>PAGE</u>
1	LANN Unsteady Test Cases for Computations	5
2	Coordinates of the LANN Wing Model (Section 3, $\eta = 0.475$, Local Chord = 258.06 mm)	7
3	Equivalent 2-d Flow Conditions for Matched Theoretical and Experimental Pressusre Distributions on Wing Section 3	9

LIST OF SYMBOLS

[A]	matrix of unsteady aerodynamic influence coefficients
b	shift of aerodynamic center due to 3-d effects, $b = b' + ib''$ (Eq. 4)
c	chord
[C]	matrix of sectional unsteady aerodynamic coefficients
C_{m_i}	sectional unsteady moment coefficient, $C_{m_i} = C'_m + iC''_m$ (relative to 0.25 c, positive nose down)
C_{M_i}	wing unsteady moment coefficient, $C_{M_i} = C'_M + iC''_M$ (relative to 0.25 c_{MAC} , positive nose down)
c_{MAC}	mean aerodynamic chord, $c_{MAC} = 0.268 m$
C_{p_i}	unsteady pressure coefficient, $C_{p_i} = C'_p + i C''_p$
C_{p_m}	(mean) steady pressure coefficient
c_r , CR	root chord
c_t	tip chord
C_{z_i}	sectional unsteady lift coefficient, $C_{z_i} = C'_z + i C''_z$
C_{Z_i}	wing unsteady lift coefficient, $C_{Z_i} = C'_Z + i C''_Z$
C_Z	wing steady lift coefficient
f, F	frequency (Hz)
k, K	reduced frequency based on semi-chord, $k = \pi cf/U_\infty$
k	unsteady sectional lift coefficient for unit motion, $k = k' + i k''$ (Eq. 2)
m	unsteady sectional moment coefficient for unit motion, $m = m' + i m''$ (Eq. 3)
M_∞ , MACH, MA	free-stream Mach number
[q]	matrix of amplitudes of sectional pitch and heave motions along wing span
Re, RE	Reynolds number
s	semi-span (m)
S	surface of semi-span wing (m^2)
t/c	thickness-to-chord ratio
U_∞	free-stream velocity

LIST OF SYMBOLS (cont'd)

x	streamwise coordinate
x_t	location of transition strip
y_{MAC}	spanwise coordinate of c_{MAC}
z	coordinate normal to x and y coordinates
α_m , ALFA, ALPHA	(mean) angle of attack (deg)
α_1 , DALFA	amplitude (deg)
η	spanwise coordinate, $\eta = y/s$
$\Lambda_{0.25}$	sweep angle of quarter-chord line (deg)

Superscripts

S	subsonic theory
T	transonic theory

Subscripts

e	equivalent 2-d (for swept wing)
---	---------------------------------

During the first part of the cooperative program of GELAC, AFWAL, NASA-Langley and NLR, unsteady transonic pressure measurements were performed on a semi-span wind-tunnel model of a transport-type supercritical wing, oscillating in pitch (Ref. 1). The model, of which the geometry is similar to that of wing A designed by GELAC (Ref. 2), has become known as the LANN model. During the second part, correlations of experimental data and analytical results from calculations were to be made by both GELAC and NLR. Eight test cases with attached flow were selected, covering influences of Mach number, frequency and mean angle of attack.

The present report contains a description of the correlation made by NLR and presents the results.

The computational method used by NLR is the so-called quasi-3-d (Q3D) method, which combines 2-d unsteady transonic small perturbation theory (the LTRAN2-NLR computer program, Ref. 3) with 2-d and 3-d subsonic Doublet Lattice methods according to the quasi-3-d concept (Ref. 4). This engineering-type method was developed in particular for applications in flutter calculations for high aspect ratio wings. A first application to a supercritical wing was reported in reference 5.

In this report, a summary of the LANN model measurements is described in section 2. An outline of the Q3D method is given in section 3. The computations and results are discussed in sections 4 and 5, respectively.

The experimental data were obtained in the NLR 2 x 1.6 m² transonic windtunnel (HST). The model was designed and built by GELAC. During the test it was mounted at the wind-tunnel side wall and could pitch about an axis normal to the wall through 62 % of the root chord (Fig. 1)*. Mean steady and unsteady pressure measurements were carried out at six streamwise sections, using many pressure tubes connected with scanning valves and a limited number of pressure transducers mounted flush with the model surface (Fig. 2). In four other sections accelerometers were mounted to measure the amplitude distribution of the oscillating wing. The Mach number was varied between 0.62 and 0.95 at three angles of attack,

*Figures are located at end of report.

covering a considerable part of the transonic flight regime (Fig. 3). The Reynolds number was approximately 5×10^6 , based on the mean aerodynamic chord. A transition strip was fixed at $0.05 c_{MAC}$ downstream of the nose. The reduced frequency was varied between $k = 0$ and 0.3 ($f = 0$ to 72 Hz), the amplitude was $\alpha_1 = 0.25$ deg in most cases. As the lowest natural frequency of about 30 Hz, corresponding to fundamental wing bending, was well within the measuring range, the vibration modes were strongly dependent on the frequency (Fig. 4). The experimental results are available in reference 1 as unsteady pressure distributions, sectional lift and moment coefficients, overall lift and moment coefficients and normalized vibration modes.

In view of the correlation in section 5 of measured and calculated lift and moment coefficients, some remarks are made here on the accuracy of the experimental values. Due to a number of inoperative pressure holes, the integrated airloads may not provide an accurate approximation of the real airloads in various sections. In each section one or two pressure holes are inoperative in the first half of the sectional chord. For flow conditions where the shock wave is close to the inoperative pressure holes, the unsteady pressure peaks have not been measured accurately. Further, inoperative pressure holes are also located in the nose region at the lower side of sections 5 and 6. All this missing information about the unsteady pressure distributions may have serious repercussions for both lift and moment coefficients and may lead to unrealistic effects of the vibration amplitudes on these airloads.

3 THE COMPUTATIONAL METHOD

The computational method used at NLR, the so-called quasi-3-d (Q3D) method (Ref. 4) is of an engineering type and has been developed in particular for use in transonic flutter calculations (Ref. 5). The method is assumed to be applicable for high aspect ratio wings for which spanwise gradients in the wing loading are small over a considerable part of the wing span. The method essentially provides spanwise distributions of unsteady lift and moment in which both the effects of finite span and wing thickness are taken into account. The Q3D method is based on the combination of three methods:

- 2-d and 3-d Doublet-Lattice methods to compute subsonic 2-d and 3-d sectional unsteady airloads,
- a 2-d transonic method to compute 2-d sectional unsteady airloads including the effects of the mean steady flow field and of shock wave motions. At NLR the commonly used method is the LTRAN2-NLR code (Ref. 3) which solves the low frequency transonic small perturbation potential equation. Recently also a viscous version has become available (LTRANV program, Ref. 6) which combines the LTRAN2-NLR code with the lag-entrainment method of Green for a steady turbulent boundary layer.

Spanwise distributions of unsteady airloads are computed as follows (Fig. 5):

- a. The wing is divided into a number of streamwise strips.
- b. The 3-d Doublet-Lattice method is used to compute sectional unsteady airloads for unit pitch and heave motions of each strip. The results form a matrix $[A_{3D}^S]$ of subsonic 3-d aerodynamic influence coefficients (AIC's);
- c. A diagonal matrix $[A_{2D}^S]$ of subsonic 2-d AIC's is generated using results of a 2-d Doublet-Lattice method for unit pitch and heave motions of each strip, taking into account the spanwise variation of reduced frequency based on the local semi-chord. The equivalent 2-d conditions are derived from the 3-d streamwise conditions using the well-known equivalence rules for a swept wing. The calculated unsteady airloads are transformed back to quantities based on the 3-d streamwise conditions.
- d. Analogous to the subsonic 2-d computations, a similar matrix $[A_{2D}^T]$ of transonic 2-d AIC's is generated using results of a 2-d transonic theory. In order to reduce computational cost, transonic flow computations are usually carried out for one representative wing section (for the LANN wing, section 3 at 47.5 % of the span). The initial steady flow conditions for the unsteady transonic flow computations are chosen such that the computed sectional mean steady pressure distribution can be matched satisfactorily to the experimental distribution, taking due account of the shock wave location. The approximation made by neglecting the variation of the mean steady pressure distributions over the wing span is considered to be reasonable in view of the approximative nature of the various steps in the Q3D method.

- e. The results are combined into a matrix of AIC's for the 3-d transonic unsteady airloads as follows:

$$\begin{bmatrix} A_{3D}^T \end{bmatrix} = \begin{bmatrix} A_{3D}^S \end{bmatrix} \begin{bmatrix} A_{2D}^S \end{bmatrix}^{-1} \begin{bmatrix} A_{2D}^T \end{bmatrix}. \quad (1)$$

The right-hand side of Eq (1) describes in a condensed notation the following correction procedure for the sectional unsteady lift and moment coefficients due to unit motion:

$$k_{ij_{3D}}^T = k_{ij_{2D}}^T \cdot k_{ij_{3D}}^S / k_{jj_{2D}}^S \quad (2)$$

$$m_{ij_{3D}}^T = (m_{jj_{2D}}^T + b_{ij} k_{jj_{2D}}^T) k_{ij_{3D}}^S / k_{jj_{2D}}^S \quad (3)$$

where b is the shift of the aerodynamic center due to 3-d effects:

$$b_{ij} = m_{ij_{3D}}^S / k_{ij_{3D}}^S - m_{jj_{2D}}^S / k_{jj_{2D}}^S. \quad (4)$$

- f. Expressing the spanwise variation of the vibration modes in a matrix $[q]$, the distributions of lift and moment coefficients $[C^T]$ are given by:

$$\begin{bmatrix} C^T \end{bmatrix} = \begin{bmatrix} A_{3D}^T \end{bmatrix} \begin{bmatrix} q \end{bmatrix}. \quad (5)$$

- g. Approximate 3-d sectional transonic pressure distributions are obtained by multiplying the 2-d transonic results for the local motion by the local ratio of 3-d to 2-d subsonic unsteady lift coefficients.

A program of eight computational test cases was agreed with GELAC. This program is presented in table 1. The corresponding experimental data, together with definitions and sign conventions are derived from reference 1 and included in Appendix A. The mean steady state conditions are a subsonic case and three transonic cases. An impression of the types of flow is given in figure 6 by the steady pressure distributions on a

TABLE 1
LANN unsteady test cases for computations

Run nr.	M_∞	α_m (deg)	C_Z	f (Hz)	k	α_1 (deg)	effect of:			
							M_∞	α_m	k	α_1
22	0.62	0.6	0.28	24	0.099	0.25				
24	0.62	0.6	0.28	48	0.199	0.25				
118	0.77	0.6	0.30	24	0.080	0.25				
124	0.77	2.6	0.48	24	0.080	0.25				
126	0.77	2.6	0.48	48	0.160	0.25				
73	0.82	0.6	0.32	24	0.076	0.25				
79	0.82	0.6	0.32	24	0.076	0.5				
85	0.82	0.6	0.32	48	0.151	0.25				

representative wing section (no 3 at 47.5 % semi-span). The eight unsteady flow test cases were selected as representative for the measured effects of Mach number, frequency, mean angle of attack and amplitude. Because the theoretical methods investigated are applicable to attached flow, no conditions with separated flow were selected.

The unsteady airloads were computed with the 3-d subsonic Doublet-Lattice method as well as the transonic Q3D method. Both sets of results are presented in this report. In the latter method, the 2-d transonic unsteady flow computations for section 3 were carried out using the inviscid LTRAN2-NLR code and, for one case, also the viscous LTRANV code. The streamwise coordinates of section 3 are listed in table 2. For the equivalent 2-d computations, the z-coordinates were smoothed and scaled by the equivalence rule for a swept wing ($z_e = z / \cos \Lambda$). The transonic unsteady pressure, lift and moment coefficients (C_{p_i} , C_{z_i} and C_{m_i} , defined in Appendix A) were derived from the first harmonic components of the computed results of the second cycle of a sinusoidal oscillation. Higher harmonics were very small, except near shock waves.

The unsteady computations were complicated by the fact, mentioned in section 2, that the measured vibration mode varies with frequency and, though less strongly, with the mean steady state conditions (Fig. 4). Also, each measured vibration mode had out-of-phase components. In the present computations both effects were taken into account. The effect of the out-of-phase component, however, appeared to be small in all cases considered.

In addition to the unsteady flow computations, also quasi-steady airloads were computed for each mean steady state. A comparison with quasi-steady experimental data gives a useful supplement to the unsteady results, because no errors associated with the tube transfer functions and the measurement of the vibration mode are introduced.

TABLE 2

Coordinates of the LANN wing model section 3

 $(\eta = 0.475, \text{Local chord} = 258.06 \text{ mm})$

upper side				lower side							
x/c	z/c	x/c	z/c	x/c	z/c	x/c	z/c	x/c	z/c	x/c	z/c
0.00000	0.01001	0.02822	0.03617	0.00000	0.01001	0.04299	-0.02058	0.91418	-0.01005		
0.00003	0.01043	0.03114	0.03717	0.00008	0.00569	0.04542	-0.02130	0.93438	-0.00963		
0.00039	0.01308	0.03310	0.03784	0.00018	0.00515	0.04798	-0.02206	0.94849	-0.00974		
0.00053	0.01281	0.03566	0.03868	0.00048	0.00394	0.05045	-0.02275	0.96149	-0.01006		
0.00089	0.01466	0.03851	0.03957	0.00088	0.00305	0.05315	-0.02349	0.96965	-0.01042		
0.00133	0.01589	0.04086	0.04025	0.00100	0.00282	0.05785	-0.02477	0.97750	-0.01089		
0.00166	0.01658	0.04347	0.04095	0.00143	0.00203	0.06279	-0.02605	0.98324	-0.01133		
0.00204	0.01741	0.04668	0.04176	0.00172	0.00142	0.06792	-0.02736	0.98728	-0.01169		
0.00229	0.01784	0.04886	0.04227	0.00210	0.00083	0.07281	-0.02852	0.99289	-0.01224		
0.00267	0.01855	0.05101	0.04276	0.00255	0.00014	0.07745	-0.02963	0.99588	-0.01255		
0.00313	0.01933	0.05309	0.04321	0.00278	-0.00002	0.08323	-0.03098	1.00000	-0.01298		
0.00338	0.01943	0.05520	0.04365	0.00328	-0.00078	0.08734	-0.03188				
0.00384	0.02013	0.05646	0.04392	0.00345	-0.00090	0.09256	-0.03303				
0.00438	0.02105	0.05776	0.04416	0.00391	-0.00150	0.09715	-0.03402				
0.00476	0.02150	0.06279	0.04512	0.00429	-0.00192	0.10215	-0.03507				
0.00494	0.02164	0.06762	0.04593	0.00469	-0.00237	0.10725	-0.03613				
0.00533	0.02207	0.07253	0.04670	0.00525	-0.00284	0.11690	-0.03807				
0.00563	0.02248	0.07749	0.04739	0.00560	-0.00326	0.12674	-0.03999				
0.00619	0.02312	0.08732	0.04861	0.00615	-0.00386	0.13650	-0.04185				
0.00657	0.02339	0.09770	0.04975	0.00644	-0.00412	0.14639	-0.04366				
0.00698	0.02392	0.10686	0.05065	0.00652	-0.00404	0.15625	-0.04541				
0.00723	0.02407	0.11705	0.05152	0.00716	-0.00483	0.16622	-0.04709				
0.00766	0.02469	0.12658	0.05226	0.00770	-0.00531	0.17611	-0.04866				
0.00821	0.02522	0.15216	0.05387	0.00815	-0.00563	0.18594	-0.05015				
0.00853	0.02552	0.17651	0.05499	0.00861	-0.00600	0.19641	-0.05163				
0.00901	0.02593	0.20061	0.05585	0.00907	-0.00635	0.20584	-0.05289				
0.00953	0.02638	0.22548	0.05640	0.00963	-0.00675	0.21521	-0.05407				
0.00964	0.02644	0.25834	0.05683	0.01011	-0.00702	0.22575	-0.05533				
0.01004	0.02672	0.31258	0.05679	0.01069	-0.00741	0.25009	-0.05794				
0.01068	0.02730	0.37718	0.05573	0.01110	-0.00769	0.27463	-0.06020				
0.01113	0.02761	0.42746	0.05418	0.01153	-0.00794	0.29886	-0.06197				
0.01195	0.02819	0.47585	0.05201	0.01249	-0.00848	0.32343	-0.06334				
0.01251	0.02858	0.52187	0.04929	0.01355	-0.00901	0.34891	-0.06433				
0.01324	0.02908	0.57090	0.04580	0.01456	-0.00951	0.37271	-0.06495				
0.01381	0.02947	0.62482	0.04129	0.01540	-0.00990	0.39978	-0.06522				
0.01442	0.02980	0.67201	0.03658	0.01642	-0.01040	0.42228	-0.06507				
0.01492	0.03007	0.71828	0.03132	0.01739	-0.01088	0.44655	-0.06452				
0.01546	0.03040	0.77026	0.02474	0.01841	-0.01135	0.47114	-0.06361				
0.01601	0.03076	0.81917	0.01771	0.01950	-0.01187	0.49612	-0.06232				
0.01630	0.03085	0.86493	0.01053	0.02041	-0.01230	0.52041	-0.06061				
0.01687	0.03119	0.91586	0.00224	0.02144	-0.01282	0.55624	-0.05725				
0.01745	0.03155	0.92894	0.00000	0.02235	-0.01321	0.58729	-0.05374				
0.01800	0.03182	0.96489	-0.00594	0.02342	-0.01368	0.62017	-0.04935				
0.01844	0.03204	1.00000	-0.01165	0.02434	-0.01405	0.65092	-0.04474				
0.01960	0.03256			0.02537	-0.01443	0.68218	-0.03987				
0.02036	0.03292			0.02659	-0.01487	0.71732	-0.03435				
0.02129	0.03341			0.02732	-0.01517	0.75083	-0.02898				
0.02227	0.03385			0.02843	-0.01556	0.76832	-0.02599				
0.02328	0.03426			0.03079	-0.01641	0.79117	-0.02259				
0.02428	0.03469			0.03318	-0.01719	0.81581	-0.01915				
0.02553	0.03518			0.03561	-0.01809	0.84046	-0.01603				
0.02637	0.03552			0.03810	-0.01904	0.86483	-0.01340				
0.02731	0.03587			0.04044	-0.01979	0.88946	-0.01136				

5.1 Steady pressure distributions

In figure 6 the computed mean pressure distributions in section 3 are compared with experimental results. To obtain a reasonable matching of theoretical and experimental results, the theoretical angles of attack differ from the experimental values. This is shown in table 3, where the equivalent 2-d values of M_∞ and α_m used in the computations are compared with the experimental 3-d values. With increasing Mach number, the theoretical incidence has to be decreased, to prevent the shock wave from moving too far downstream. In addition to the neglect of 3-d effects and viscous effects, the used small perturbation theory may explain this phenomenon.

As a result of the matching procedure, a reasonable agreement is obtained between theoretical and experimental results. The calculated values at the rear part of the chord are overpredicted due to the neglect of viscous effects. In the transonic results the pressure level in the supersonic flow region and, consequently, the strength of the shock wave are underpredicted. This also points to shortcomings of the small perturbation theory.

5.2 Unsteady airloads as function of Mach number

5.2.1 Quasi-steady results

In figures 7 to 10 quasi-steady results are presented for $M_\infty = 0.62$, 0.77 and 0.82 at $\alpha_m = 0.6$ deg. The corresponding mean steady pressure distributions are shown in figure 6a, b and c.

Pressure distributions: Figure 7 presents the quasi-steady pressure distributions. The theoretical results give a good qualitative prediction of the development and downstream displacement of the shock pressure peak, with increasing Mach number. In the subsonic case a good agreement with experiment exists except for the nose region, where much higher pressure peaks are predicted. With increasing Mach number the pressure level on the front half of the airfoil is increasingly overpredicted. This may be largely due to the small perturbation assumption underlying the 2-d transonic theory, as well as to the neglect of viscous effects.

It should be noted that the experimental results at $M_\infty = 0.77$ were obtained for an amplitude of $\alpha_1 = 1$ deg, which leads to a lower and wider pressure peak than for $\alpha_1 = 0.25$ deg. This effect of amplitude is very

TABLE 3
Equivalent 2-d flow conditions for matched theoretical and
experimental pressure distributions on wing section 3

Run nr.	M_{∞}	α_m (deg)	$M_{\infty e}$ ($=M_{\infty} \cos \Lambda$)	α_{me} (deg)
22, 24	0.62	0.6	0.562	0.5
118	0.77	0.6	0.698	0
124, 126	0.77	2.6	0.698	0.75
73, 79, 85	0.82	0.6	0.743	-0.25

clearly illustrated for $M_\infty = 0.82$, where the most significant changes in pressure (occurring at the shock peak) are shown.

Sectional coefficients: The spanwise distributions of quasi-steady lift and moment coefficients are shown in figures 8 and 9.

In the subsonic case ($M_\infty = 0.62$) the computed effect of thickness on the lift coefficient is small, as expected, and consists of a small increase of C'_z . The level of C'_z is overpredicted, which can be largely attributed to the neglect of viscous effects. The sectional moments are predicted very well.

With increasing Mach number, the computed steady flow effects in C'_z also increase. This can be associated with the development of shock waves and the increased extent of the supersonic flow region, as shown for section 3 in figure 6a, b and c. Although the experimental results also exhibit a stronger effect of Mach number on C'_z than predicted by subsonic theory, the level of C'_z is increasingly overpredicted by the transonic method. A correction for the effect of boundary layer and wake for section 3 at $M_\infty = 0.82$ (Figs 8 and 9), computed with the LTRANV program, partly explains the overprediction of C'_z .

With increasing Mach number also the shape of the spanwise distribution of C'_z is predicted with decreasing accuracy. The experimental results indicate a relatively strong influence of Mach number on the unsteady airloads between 30 and 70 % of the semi-span. The theoretical results, however, show a typical subsonic distribution of which only the level is affected by increasing Mach number. The disagreement compared to the transonic experimental results may indicate shortcomings of the subsonic 3-d correction procedure in the Q3D method.

Drawing a definite conclusion about the accuracy of the Q3D method, however, is difficult because of the inaccuracy in the integration of the experimental pressure distributions, as mentioned in section 2. This is also true for the effect of amplitude on the experimental results, which is illustrated in figures 7 and 8 for $M_\infty = 0.82$. Increasing the amplitude from $\alpha_1 = 0.25$ to 1 deg leads to different distributions of quasi-steady airloads which are, probably by coincidence, quite similar to the results of subsonic theory.

The sectional moment coefficients (Fig. 9) are not predicted more accurately in a quantitative sense, by accounting for transonic effects. However, in a qualitative sense the Q3D method correctly predicts the tendency to more negative (nose up) moment coefficients at $M_\infty = 0.77$, and to more positive (nose down) values at $M_\infty = 0.82$. This tendency is

explained by the contribution of the shock wave to C'_m , which is upstream of the quarter-chord point at $M_\infty = 0.77$ and downstream of this point at $M_\infty = 0.82$ (Figs 6b and c). Unlike the lift coefficient, the moment coefficient in section 3 is not improved by applying a viscous correction (Fig. 9, $M_\infty = 0.82$). A comparison with more refined calculation methods is necessary to determine to what extent the small perturbation assumption and the quasi-3-d concept are responsible for the observed differences.

Overall coefficients: The above observations are, of course, also reflected in the overall coefficients in figure 10. It should be noted that the overall moment is not an average of the sectional moments, as it is defined relative to an axis through the quarter-chord point of the mean aerodynamic chord, normal to the free stream.

5.2.2 Unsteady results for $f = 24$ Hz

Unsteady results at a mean incidence of $\alpha_m = 0.6$ deg and a frequency of $f = 24$ Hz are shown in figures 11 to 14.

Pressure distributions: The unsteady pressure distributions at $f = 24$ Hz (Fig. 11) show the same order of agreement between experimental and theoretical results as in the quasi-steady case. In a quantitative sense, the agreement is slightly better. The computed imaginary parts show clearly the increasing influence of the shock wave if the Mach number is increased.

For $M_\infty = 0.82$ the computed effect of amplitude was investigated. In figure 11 the significant changes in pressure are indicated, which occur only at the shock wave pressure peaks. The Q3D method predicts both a reduction and a slight widening of the peak. The experimental results exhibit only a reduction of the pressure peaks. Here, the spacing of the pressure holes does not provide sufficient resolution to indicate a widening of the peak, which is still likely to be present in reality as in the quasi-steady case. As a result the computed sectional airloads, discussed below, are not significantly affected by the increase of amplitude, in contrast with the experimental results which are strongly dependent on such a change. This example illustrates very distinctly the remarks in section 2 on the experimental accuracy in relation with the spacing of the pressure holes.

Sectional coefficients: The spanwise distributions of unsteady lift and moment coefficients are shown in figures 12 and 13, respectively.

The lift coefficient C'_z behaves very much like the quasi-steady case, although the computed effect of transonic flow is smaller. The agreement between the theoretical and experimental results is better, in spite of some difference in the theoretical and experimental spanwise distributions of C'_z .

The computed transonic effects on C''_z increase with Mach number. The shift of C''_z to more negative values is correctly predicted by the Q3D method. Although the experimental values are somewhat underpredicted, a significant improvement has been obtained compared to subsonic theory.

For $M_\infty = 0.82$ the effect of an increase in amplitude to $\alpha_1 = 0.5$ deg is indicated for the experimental data; in the computed results this effect is negligible.

Also the distribution of C'_m (Fig. 13) shows the same tendency as in the quasi-steady case (Fig. 9). The computed steady flow effects yield a more positive value of C''_m at transonic conditions, which is also found in the experimental data. In spite of this qualitative improvement relative to linear theory, C''_m is not predicted more accurately by the Q3D method. The overprediction can be associated with the overprediction of the unsteady pressures in the front part of the airfoil (Fig. 11).

For section 3 at $M_\infty = 0.82$ a correction for viscous effects was computed using the LTRANV computer program. The resulting reduction of C'_z and C'_m (Figs 12, 13) is similar too, but smaller than that in the quasi-steady case. The effect on the imaginary part is a positive shift, which causes a larger difference relative to the experimental results. This again points to shortcomings of the inviscid flow computation, related to the small perturbation assumption and the quasi-3-d concept.

Overall coefficients: The overall unsteady lift and moment coefficients for $f = 24$ Hz, shown in figure 14, expectedly reflect the behaviour of the sectional airloads discussed so far. The strong variation of the experimental unsteady airloads above $M_\infty = 0.82$ is due to flow separation, which is out of the scope of this report.

5.2.3 Unsteady results for $f = 48$ Hz

The differences between the results for $f = 24$ Hz and 48 Hz are caused both by the frequency and the vibration mode. The change of the vibration mode with frequency has been discussed already in section 2. The unsteady results for 48 Hz are shown in figures 15 to 18 for a subsonic ($M_\infty = 0.62$) and a transonic ($M_\infty = 0.82$) case.

Pressure distributions: The unsteady pressure distributions on section 3 (Fig. 15) show a similar development with Mach number as already discussed for $f = 24$ Hz.

Sectional coefficients: Accounting for transonic effects leads again to an increased overprediction of C'_z and to a better prediction of C''_z (Fig. 16). The maximum values of the experimental lift coefficients at $M_\infty = 0.82$, which occur between 30 and 70 % of the semi-span like in the quasi-steady case, are not well predicted.

The experimental moment coefficients (Fig. 17) are predicted surprisingly well in the subsonic case. Apparently the errors due to the neglect of viscous effects and to the approximations in the inviscid theory cancel out here. In the transonic case, the Q3D method gives a good prediction of the transonic effects on C'_m , which are not predicted by subsonic theory. On the other hand, the Q3D method overpredicts C''_m at $M_\infty = 0.82$.

Overall coefficients: The overall unsteady airloads for $f = 48$ Hz (Fig. 18) show a behaviour which is quite similar to that at $f = 24$ Hz.

5.3 Unsteady airloads as function of frequency

From the results for $\alpha_m = 0.6$ deg presented in the previous sections it can be derived that the effect of frequency is reasonably well predicted by the Q3D method. To illustrate this effect more clearly, unsteady results will also be presented for various frequencies, for a mean incidence of $\alpha_m = 2.6$ deg, at $M_\infty = 0.77$. (Figs 19 to 22). The results correspond to the mean steady state shown in figure 6d. Again, it should be noted that also the vibration mode varies with frequency.

Pressure distributions: The quasi-steady and unsteady pressure distributions on section 3 shown in figure 19 exhibit an increasing agreement between theory and experiment at increasing frequency. In particular the decrease of the real part, and the increase of the imaginary part of the pressure peak at the shock wave is well predicted.

Sectional coefficients: The unsteady airloads are shown in figures 20 and 21. In particular the experimental distributions of C'_z and C''_z (Fig. 20) show strong variations over the wing span, which are likely due to the experimental inaccuracy discussed in section 3. The nature and accuracy of the computed distributions is rather similar to that of the previous cases, and need not be discussed further.

Overall coefficients: The development of the overall unsteady airloads, shown in figure 22, reflects the global accuracy of the Q3D method and demonstrates that the merit of this method is the improved accuracy of the computed imaginary part of the unsteady lift. Note the discontinuity indicated at $k = 0.1$, which corresponds to the natural frequency of the first wing bending mode.

5.4 Unsteady airloads as function of mean angle of attack

The effect of mean angle of attack is investigated for $M_\infty = 0.77$ at $f = 24$ Hz. The steady state pressure distributions are shown in figures 6c ($\alpha_0 = 0.6$ deg) and 6d ($\alpha_0 = 2.6$ deg). The results for these cases are already discussed separately in the previous sections.

Pressure distributions: The computed pressure distributions (Fig. 23) predict correctly the increase and downstream displacement of the shock wave pressure peaks with increasing incidence.

Sectional coefficients: The computed distributions of C'_z (Figs 24 and 25) show an increase, while C''_z becomes more negative at larger angle of attack. The distributions of C'_m and C''_m shift slightly to larger values, due to the nose-down contribution of the more downstream positioned shock wave. The above effects of incidence are not clearly present in the experimental results, except for the behaviour of C'_z and C''_z at section 3.

Overall coefficients: The effect of incidence on the overall airloads is shown in figure 26. The slight effect of incidence on the results of subsonic theory is due to a small variation of the vibration mode. The increase of the unsteady airloads with increasing incidence, as predicted by the Q3D method, only agrees with the experimental results for C'_z and C''_M . In a quantitative sense, only C''_z is predicted satisfactorily, as before.

Experimental data for the LANN supercritical wing model oscillating in pitch have been used for verification of a quasi-3-d method to compute unsteady airloads at transonic flow conditions. An outline has been given of this method, which combines 2-d transonic theory with 2-d and 3-d subsonic theory. A comparison of computed and measured results for a number of attached flow conditions, covering variations of Mach number, frequency, mean angle of attack leads to the following conclusions:

- a. Accounting for the effects of transonic flow, including shock wave motions, using the quasi-3-d method does not in all respects lead to an improved prediction of experimental unsteady airloads, compared to subsonic theory.
- b. In a quantitative sense, the imaginary part of the sectional and overall lift coefficients is predicted significantly better, whereas the real part is more overpredicted. The moment coefficients are not predicted more accurately, compared to subsonic theory.
- c. The quasi-3-d method gives a qualitatively better prediction of the effects of Mach number and frequency on the unsteady lift coefficients and on the real part of the moment coefficients, compared to subsonic theory. The predicted effects of incidence on the unsteady airloads do not agree very well with the measured effects.
- d. The still existing differences between experimental data and results of the quasi-3-d method can be partly attributed to the neglect of viscous effects, to the small perturbation assumption underlying the 2-d transonic flow computations and to the subsonic 3-d corrections. On the other hand, due to a number of inoperative pressure holes the experimental lift and moment coefficients are of insufficient accuracy to draw a definite conclusion on the accuracy of the quasi-3-d method. For this reason, also the measured effect of amplitude is inconclusive.
- e. The computed effect of amplitude on the unsteady airloads on a representative wing section is very small.

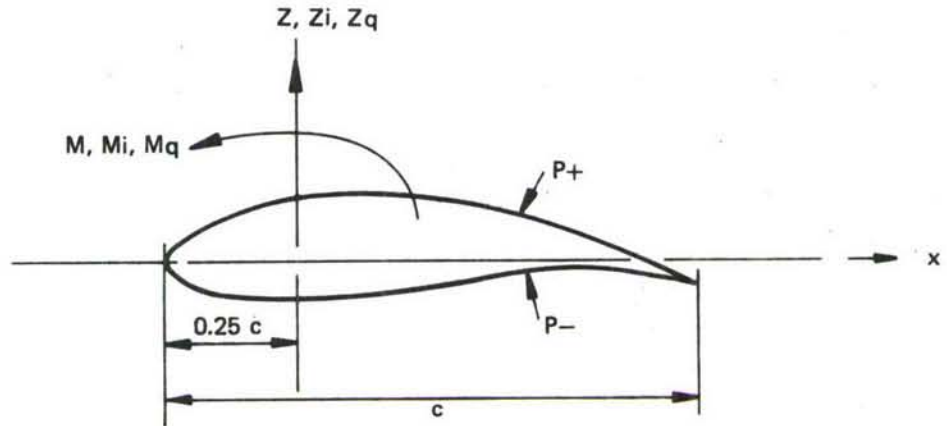
APPENDIX

EXPERIMENTAL DATA FOR THE COMPUTATIONAL TEST CASES (SEE TABLE 1)

CONTENTS

	Page
A.1 Definitions and Sign Conventions	17
A.2 Sectional and Overall Airloads (Tables)	20
A.3 Pressure Distributions (Figures)	23

A.1 Definitions and sign conventions (taken from reference 1)



Note: Coefficients derived from the zeroth harmonic component of unsteady pressure signals, are indicated simply as "steady" coefficients instead of "mean" coefficients. For a pure sinusoidal signal, there is principally no difference between steady and mean coefficients.

Steady

Steady pressure coefficient:

$$C_{pm} = \frac{P_m - P_\infty}{q_\infty}$$

Steady sectional normal force:

$$Z = C_z q_\infty c; C_z = - \int_0^1 (C_{pm+} - C_{pm-}) d\left(\frac{x}{c}\right)$$

Steady sectional pitching moment about quarter-chord

$$M = C_m q_\infty c^2; C_m = - \int_0^1 (C_{pm+} - C_{pm-}) \left(\frac{x}{c} - 0.25\right) d\left(\frac{x}{c}\right)$$

Steady wing normal force:

$$Z_{wing} = C_Z q_\infty S; C_Z = - \frac{1}{S} \int_0^S \int_0^1 (C_{pm+} - C_{pm-}) d\left(\frac{x}{c}\right) \cdot c \cdot dy$$

Steady wing pitching moment about aerodynamic center:

$$M_{\text{wing}} = C_M \cdot q_\infty \cdot c_{AC} \cdot S; \quad C_M = - \frac{1}{S c_{AC}} \int_0^S \int_0^1 (C_{pm+} - C_{pm-}) \left(\frac{x-x_{AC}}{c} \right) d\left(\frac{x}{c}\right) c^2 \cdot dy$$

Unsteady

Unsteady pressure coefficient:

$$C_{pi} = C'_p + i C''_p = \frac{P_i}{q_\infty \cdot \alpha_i}$$

Unsteady sectional normal force:

$$Z_i = 2\pi \cdot q_\infty \cdot \frac{c}{2} \cdot C_{zi} \cdot \Delta\alpha \cdot e^{i\omega t}$$

$$C_{zi} = C'_z + i C''_z = - \frac{1}{\pi} \int_0^1 (C_{pi+} - C_{pi-}) d\left(\frac{x}{c}\right)$$

Unsteady sectional pitching moment about quarter-chord:

$$M_i = 2\pi \cdot q_\infty \cdot \left(\frac{c}{2}\right)^2 \cdot C_{mi} \cdot \Delta\alpha \cdot e^{i\omega t};$$

$$C_{mi} = C'_m + i C''_m = - \frac{2}{\pi} \int_0^1 (C_{pi+} - C_{pi-}) \left(\frac{x}{c} - 0.25\right) d\left(\frac{x}{c}\right)$$

Unsteady wing normal force:

$$Z_{i\text{wing}} = 2\pi \cdot q_\infty \cdot \frac{S}{2} \cdot C_{zi} \cdot \Delta\alpha \cdot e^{i\omega t};$$

$$C_{zi} = C'_z + i C''_z = - \frac{1}{\pi S} \int_0^S \int_0^1 (C_{pi+} - C_{pi-}) d\left(\frac{x}{c}\right) \cdot c \cdot dy$$

Unsteady wing pitching moment about aerodynamic center:

$$M_{i\text{wing}} = 2\pi \cdot q_\infty \cdot \left(\frac{c_{AC}}{2}\right) \cdot \frac{S}{2} \cdot C_{mi} \cdot \Delta\alpha \cdot e^{i\omega t};$$

$$C_{mi} = C'_M + i C''_M = - \frac{2}{\pi S c_{AC}} \int_0^S \int_0^1 (C_{pi+} - C_{pi-}) \left(\frac{x-x_{AC}}{c}\right) d\left(\frac{x}{c}\right) \cdot c^2 \cdot dy$$

Quasi-steady

Quasi-steady pressure coefficient:

$$C_{pq} = C_p' = \frac{P_q}{q_\infty \Delta\alpha}$$

Quasi-steady sectional normal force:

$$Z_q = 2\pi \cdot q_\infty \cdot \frac{c}{2} C_{Zq} \cdot \Delta\alpha ;$$

$$C_{Zq} = C'_Z = \frac{1}{\pi} \cdot \frac{C_z(\alpha_m + \Delta\alpha) - C_z(\alpha_m - \Delta\alpha)}{2\Delta\alpha}$$

Quasi-steady sectional pitching moment about quarter-chord:

$$M_q = 2\pi \cdot q_\infty \cdot \left(\frac{c}{2}\right)^2 \cdot C_{mq} \cdot \Delta\alpha ;$$

$$C_{mq} = C'_m = \frac{2}{\pi} \cdot \frac{C_m(\alpha_m + \Delta\alpha) - C_m(\alpha_m - \Delta\alpha)}{2\Delta\alpha}$$

Quasi-steady wing normal force:

$$Z_{q_{wing}} = 2\pi \cdot q_\infty \cdot \frac{S}{2} \cdot C_{Zq} \cdot \Delta\alpha ;$$

$$C_{Zq} = C'_Z = \frac{1}{\pi} \cdot \frac{C_Z(\alpha_m + \Delta\alpha) - C_Z(\alpha_m - \Delta\alpha)}{2\Delta\alpha}$$

Quasi-steady wing pitching moment about aerodynamic cent :

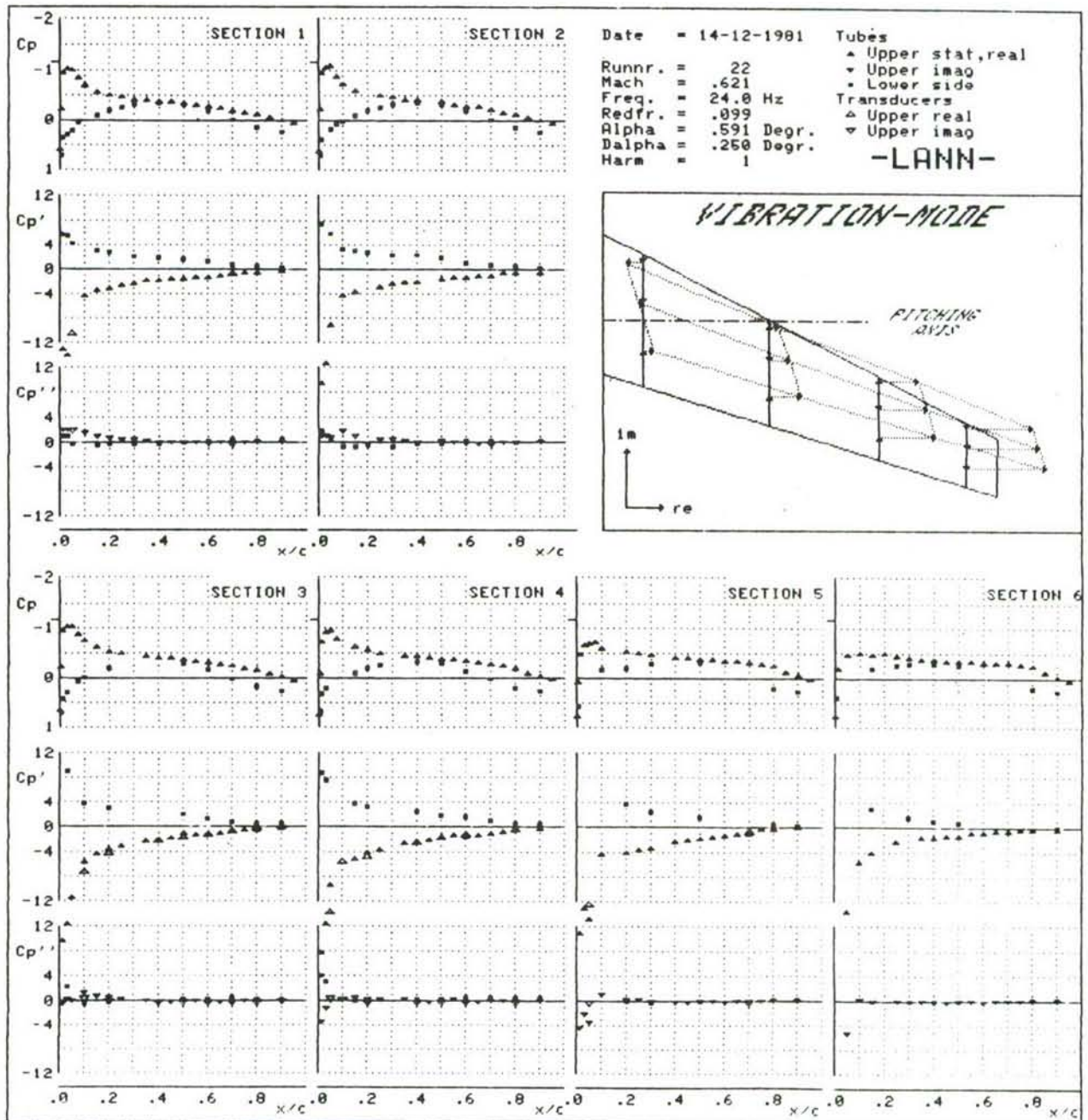
$$M_{q_{wing}} = 2\pi \cdot q_\infty \cdot \left(\frac{c_{AC}}{2}\right) \cdot \frac{S}{2} \cdot C_{Mq} \cdot \Delta\alpha ;$$

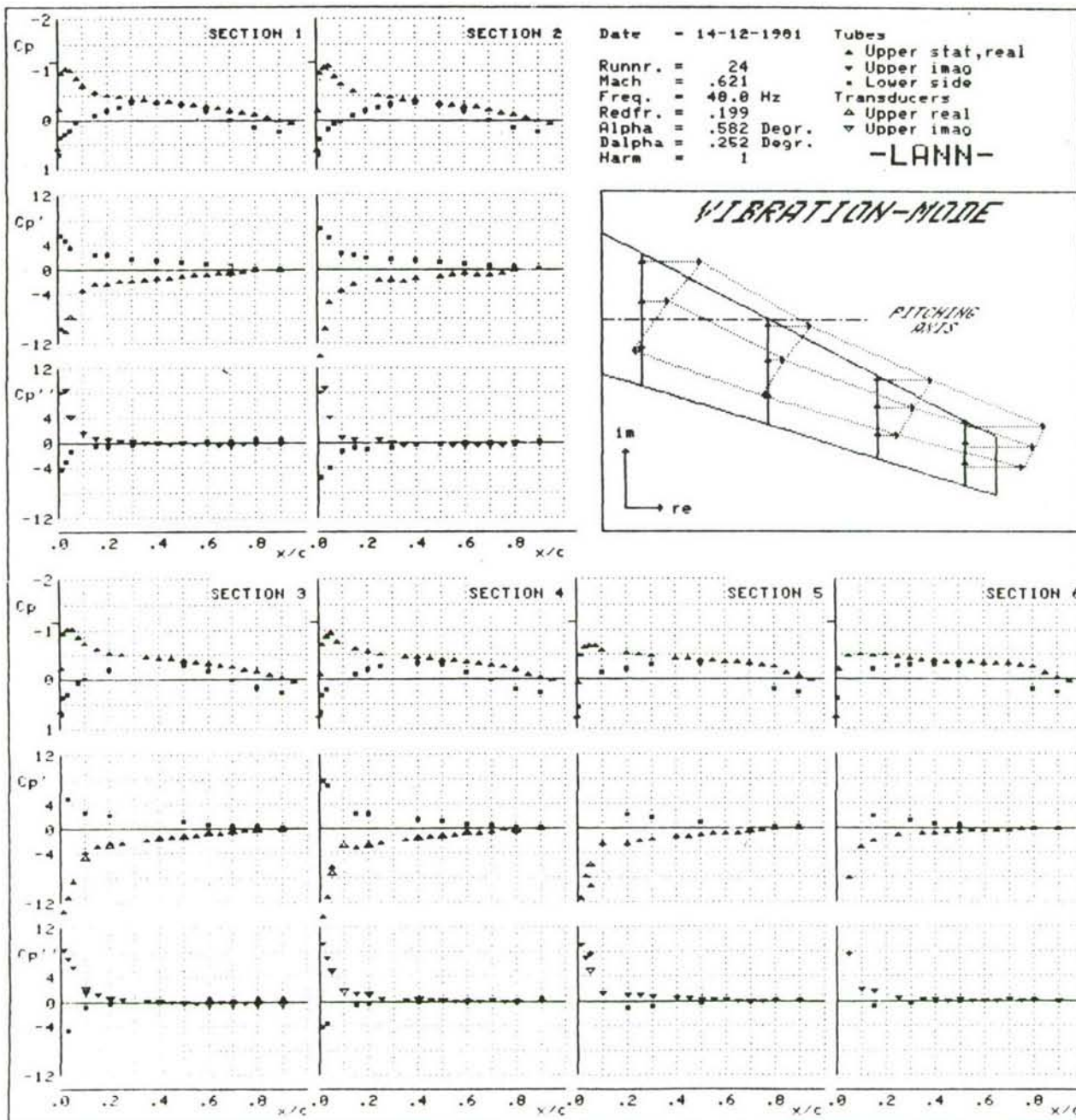
$$C_{Mq} = C'_M = \frac{2}{\pi} \cdot \frac{C_M(\alpha_m + \Delta\alpha) - C_M(\alpha_m - \Delta\alpha)}{2\Delta\alpha}$$

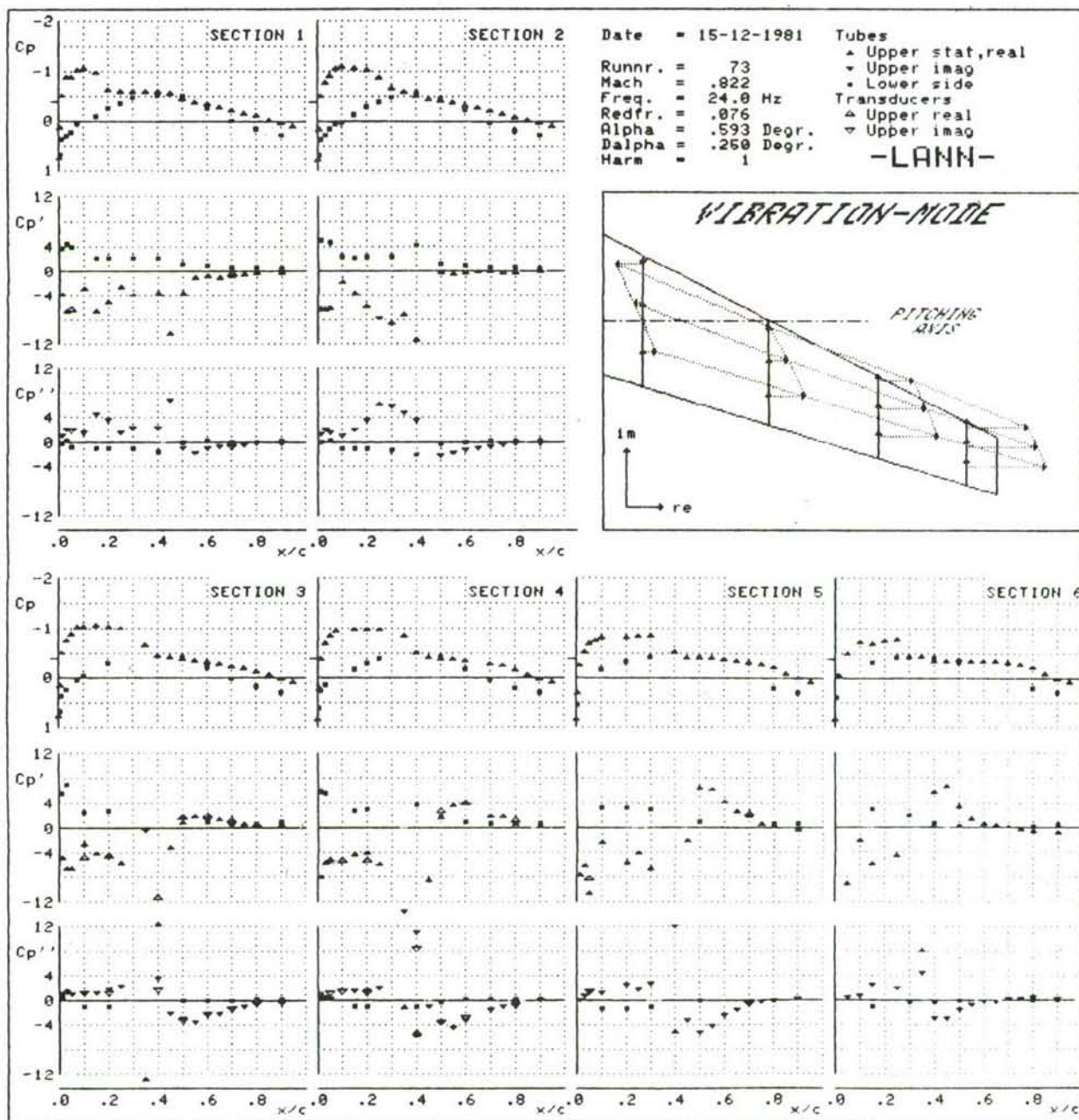
TEST CONDITIONS				NORM. COEFF.				MOM. COEFF.				DISPLACEMENTS				VIBRATION MODE			
				Cz	RE	Czi	IM	Cm	RE	Cmi	IM	REL. TO LVDT	AMPL. (-)	PHASE (DEG)		XY/(B/2)	HEAVE AT X=.224 M (MM)	PITCH (DEG)	
RUNNR.	=	22		SECT.1	.260	1.217	-.100	.015	.030	.086		LVDT	1.00	0.00		.000			
				SECT.2	.292	1.382	-.119	.020	-.012	.051		CALC. 1	1.02	1.65		.100			
ALFA	=	.59 (DEGR.)		SECT.3	.330	1.453	.035	.030	-.014	.065		ACC. 2	.26	2.34		.100	.05	.23	
MACH	=	.62		SECT.4	.331	1.646	.181	.043	-.026	.022		ACC. 3	.67	-178.94		.100			
RE*10**-6	=	4.82		SECT.5	.311	1.338	.078	.054	.024	.003		ACC. 4	.51	-174.33		.420			
Q	=	30.92 (KPA)		SECT.6	.261	.917	.129	.057	-.072	-.016		ACC. 5	1.28	-180.74		.420	.25	.24	
P-SETTL.	=	148.7 (KPA)										ACC. 6	1.92	-179.36		.420			
T-SETTL.	=	15.00		WING	.285	1.306	-.003	.042	.133	.155		ACC. 7	2.33	-178.35		.700	.62	.24	
DALFA	=	.25 (DEGR.)						(WING : CM ABOUT				CALC. 8	2.88	-180.42		.700			
FREQ.	=	24.00 (HZ)						AERODYN. CENTRE)				CALC. 9	3.35	-179.93		.700			
REDFR.	=	.10										CALC.10	3.89	-180.33		.920	.92	.25	
HARM.	=	1										ACC.11	4.29	-180.33		.920			
												ACC.12	4.70	-180.32		.920			
RUNNR.	=	24		SECT.1	.260	.916	-.190	.015	.011	.196		LVDT	1.00	0.00		.000			
				SECT.2	.291	.990	-.315	.021	-.028	.171		CALC. 1	1.34	1.43		.100			
ALFA	=	.58 (DEGR.)		SECT.3	.329	1.051	-.266	.030	-.017	.187		ACC. 2	.64	1.61		.100	.17	.21	
MACH	=	.62		SECT.4	.330	1.142	-.357	.043	-.050	.154		ACC. 3	.22	-179.79		.100			
RE*10**-6	=	4.84		SECT.5	.312	.818	-.396	.053	.009	.083		ACC. 4	.99	3.15		.420			
Q	=	31.01 (KPA)		SECT.6	.260	.524	-.287	.057	-.050	.089		ACC. 5	.40	3.63		.420	.57	.20	
P-SETTL.	=	149.1 (KPA)										ACC. 6	.14	169.92		.420			
T-SETTL.	=	15.00		WING	.284	.924	-.269	.042	.025	.094		ACC. 7	1.25	3.04		.700	1.14	.18	
DALFA	=	.25 (DEGR.)						(WING : CM ABOUT				CALC. 8	.82	4.93		.700			
FREQ.	=	48.00 (HZ)						AERODYN. CENTRE)				CALC. 9	.48	8.86		.700			
REDFR.	=	.20										CALC.10	1.82	4.22		.920			
HARM.	=	1										ACC.11	1.57	4.82		.920	1.68	.15	
												ACC.12	1.33	5.65		.920			

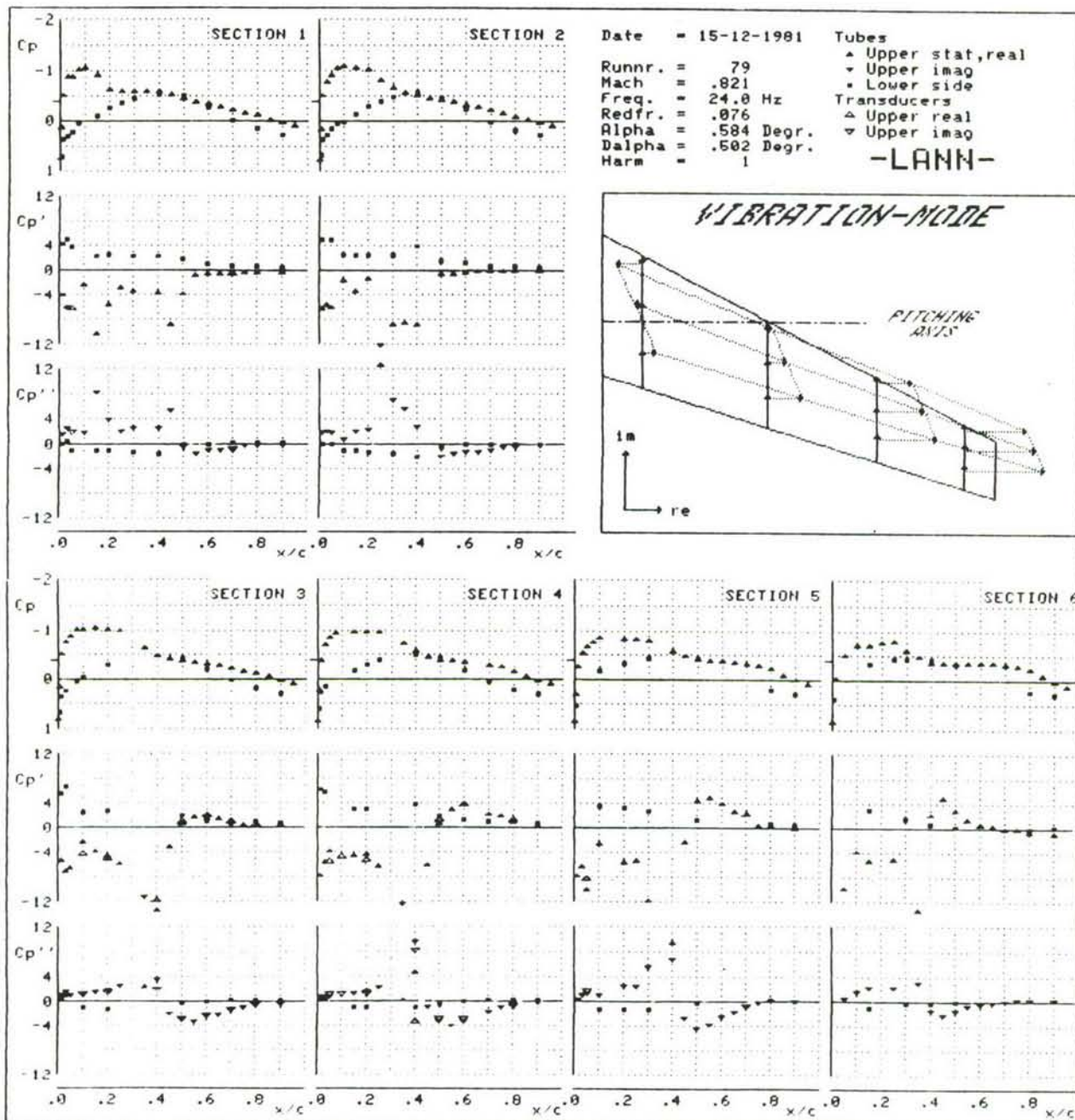
TEST CONDITIONS	NORM. COEFF.			MOM. COEFF.			DISPLACEMENTS			VIBRATION MODE		
	Cz	RE	Czi	IM	CM	RE	REL. TO LVDI	AMPL. (-)	PHASE (DEG)	REL. TO LVDI	HEAVE AT X=.224 M (MM)	PITCH (DEG)
RUNNR. = 73							LVDI	1.00	0.00			
ALFA = .59 (DEGR.)	SECT.2 .325	1.335	-.443	.014	.178	.069	CALC. 1	1.13	1.52			
MACH = .82	SECT.3 .377	2.172	-.645	.023	.147	.092	ACC. 2	.37	-.33		.01	.23
REX10**6= 5.43	SECT.4 .371	2.256	-.415	.037	.104	.127	ACC. 3	.55	-175.71			
Q =45.22 (KPA)	SECT.5 .341	1.577	-.328	.047	-.010	.113	ACC. 4	.13	-139.19			
P-SETTL. =149.1 (KPA)	SECT.6 .255	.958	-.180	.049	-.088	.047	ACC. 5	.85	-175.73		.05	.24
T-SETTL. =26.00	WING .320	1.663	-.482	.037	.367	.100	ACC. 6	1.52	-175.55			
DALFA = .25 (DEGR.)				(WING : CM ABOUT			ACC. 7	1.52	-170.87			
FREQ. =24.00 (HZ)				AERODYN. CENTRE)			CALC. 8	2.01	-174.98		.24	.23
REDFR. = .08							CALC. 9	2.50	-175.03			
HARM. = 1							CALC.10	2.61	-173.58			
							ACC.11	2.98	-174.16		.36	.22
							ACC.12	3.35	-174.61			
RUNNR. = 79							LVDI	1.00	0.00			
ALFA = .58 (DEGR.)	SECT.2 .323	1.376	-.524	.014	.156	.099	CALC. 1	1.11	1.39			
MACH = .82	SECT.3 .376	1.796	-.437	.023	.084	.132	ACC. 2	.35	-.55		.02	.46
REX10**6= 5.40	SECT.4 .362	2.074	-.460	.036	.055	.117	ACC. 3	.57	-175.93			
Q =44.88 (KPA)	SECT.5 .340	1.425	-.317	.047	-.060	.125	ACC. 4	.23	-150.27			
P-SETTL. =148.1 (KPA)	SECT.6 .262	.899	-.184	.050	-.120	.059	ACC. 5	.87	-175.58		.15	.46
T-SETTL. =26.00	WING .317	1.535	-.475	.037	.244	.161	ACC. 6	1.54	-175.82			
DALFA = .50 (DEGR.)				(WING : CM ABOUT			ACC. 7	1.56	-170.86			
FREQ. =24.00 (HZ)				AERODYN. CENTRE)			CALC. 8	2.05	-175.44		.50	.47
REDFR. = .08							CALC. 9	2.55	-175.67			
HARM. = 1							CALC.10	2.66	-174.32			
							ACC.11	3.05	-175.02		.68	.48
							ACC.12	3.44	-175.57			
RUNNR. = 85							LVDI	1.00	0.00			
ALFA = .60 (DEGR.)	SECT.2 .329	.811	-.464	.014	.173	.138	CALC. 1	1.33	1.68			
MACH = .82	SECT.3 .378	1.282	-.995	.023	.156	.122	ACC. 2	.61	2.27		.15	.21
REX10**6= 5.40	SECT.4 .374	1.300	-.777	.037	.131	.210	ACC. 3	.25	-181.47			
Q =45.07 (KPA)	SECT.5 .341	.918	-.655	.047	.046	.169	ACC. 4	.95	6.54			
P-SETTL. =148.8 (KPA)	SECT.6 .272	.576	-.411	.051	-.042	.111	ACC. 5	.34	12.94		.54	.20
T-SETTL. =27.00	WING .323	.957	-.666	.037	.266	.030	ACC. 6	.23	160.23			
DALFA = .25 (DEGR.)				(WING : CM ABOUT			ACC. 7	1.15	10.29			
FREQ. =48.00 (HZ)				AERODYN. CENTRE)			CALC. 8	.74	16.79		1.09	.18
REDFR. = .15							CALC. 9	.42	32.49			
HARM. = 1							CALC.10	1.71	12.58			
							ACC.11	1.47	15.15		1.65	.16
							ACC.12	1.22	18.81			

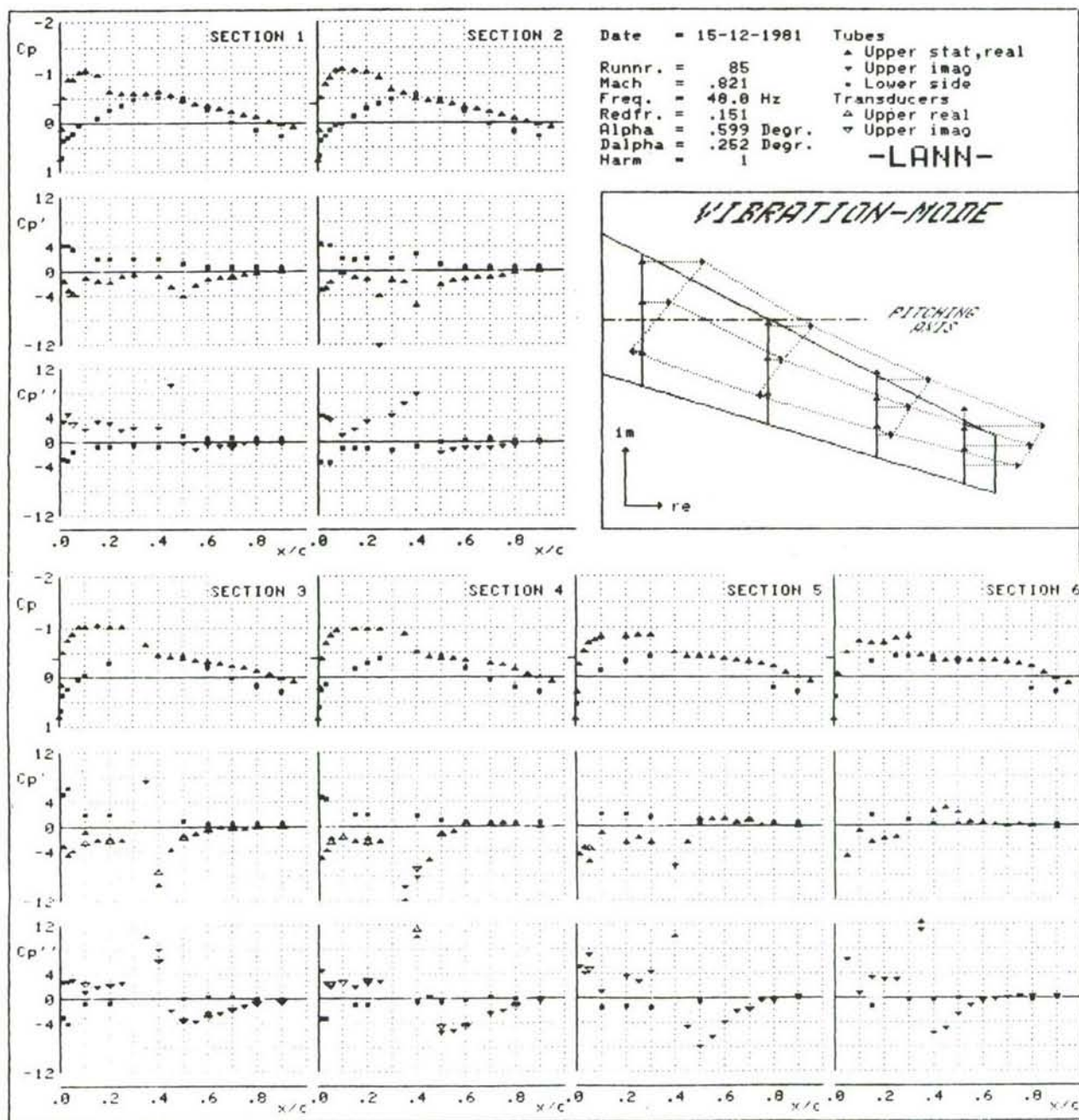
TEST CONDITIONS	NORM. COEFF.				MOM. COEFF.				DISPLACEMENTS				VIBRATION MODE			
	Cz	RE	IM	CM	RE	CM	IM	REL. TO LVD	PHASE	(-)	(DEG)	**	REL. TO LVD	PHASE	(-)	(DEG)
RUNNR. = 118																
ALFA = .60 (DEGR.)																
MACH = .77																
RE#10**=6= 5.26																
Q = 42.10 (KPA)																
P-SETTL. = 149.5 (KPA)																
T-SETTL. = 27.00																
DALFA = .25 (DEGR.)																
FREQ. = 24.00 (HZ)																
REDFR. = .08																
HARM. = 1																
RUNNR. = 124																
ALFA = 2.60 (DEGR.)																
MACH = .77																
RE#10**=6= 5.22																
Q = 41.71 (KPA)																
P-SETTL. = 148.5 (KPA)																
T-SETTL. = 27.00																
DALFA = .25 (DEGR.)																
FREQ. = 24.00 (HZ)																
REDFR. = .08																
HARM. = 1																
RUNNR. = 126																
ALFA = 2.60 (DEGR.)																
MACH = .77																
RE#10**=6= 5.21																
Q = 41.65 (KPA)																
P-SETTL. = 148.2 (KPA)																
T-SETTL. = 27.00																
DALFA = .25 (DEGR.)																
FREQ. = 48.00 (HZ)																
REDFR. = .16																
HARM. = 1																

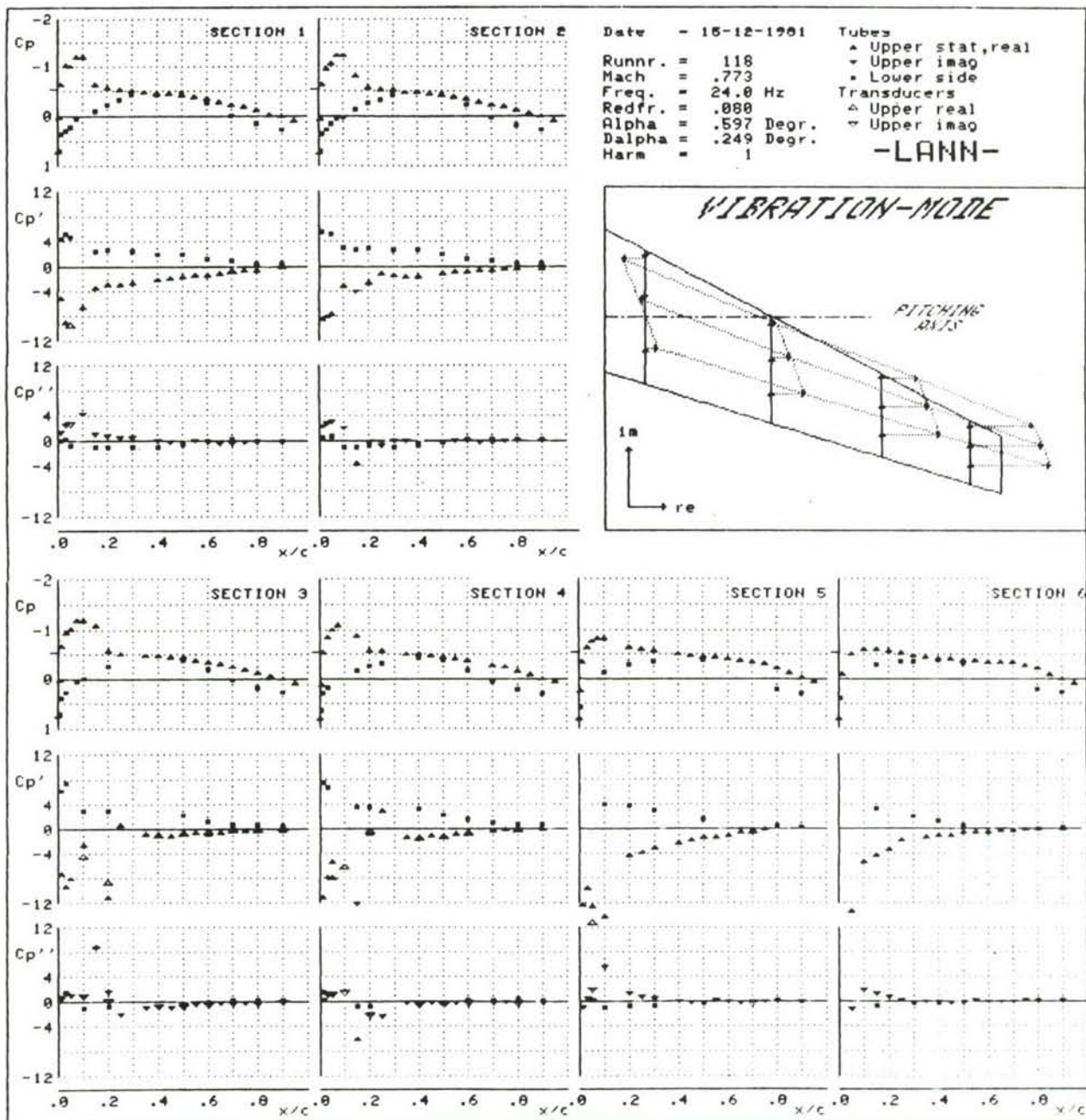


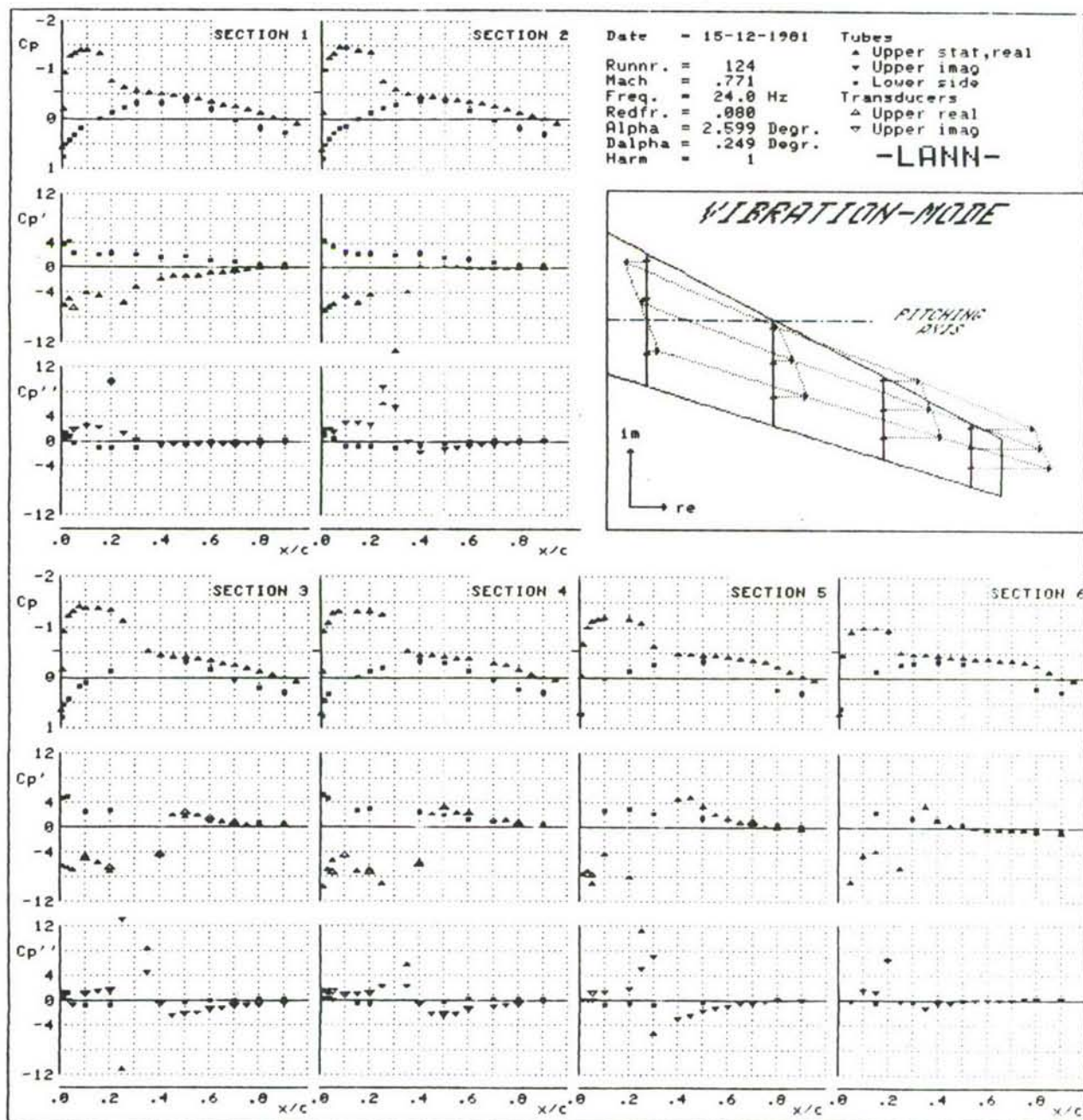


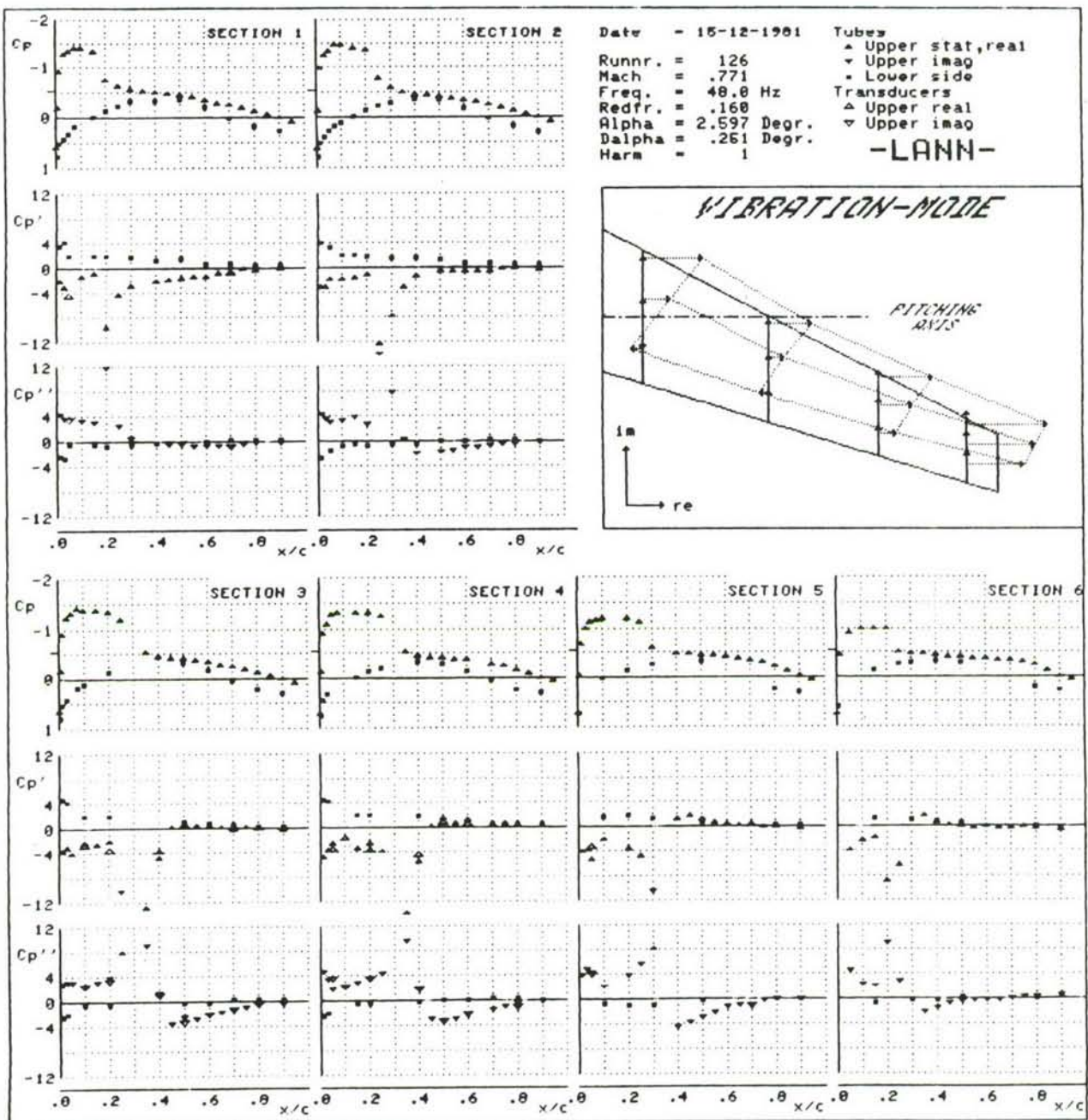












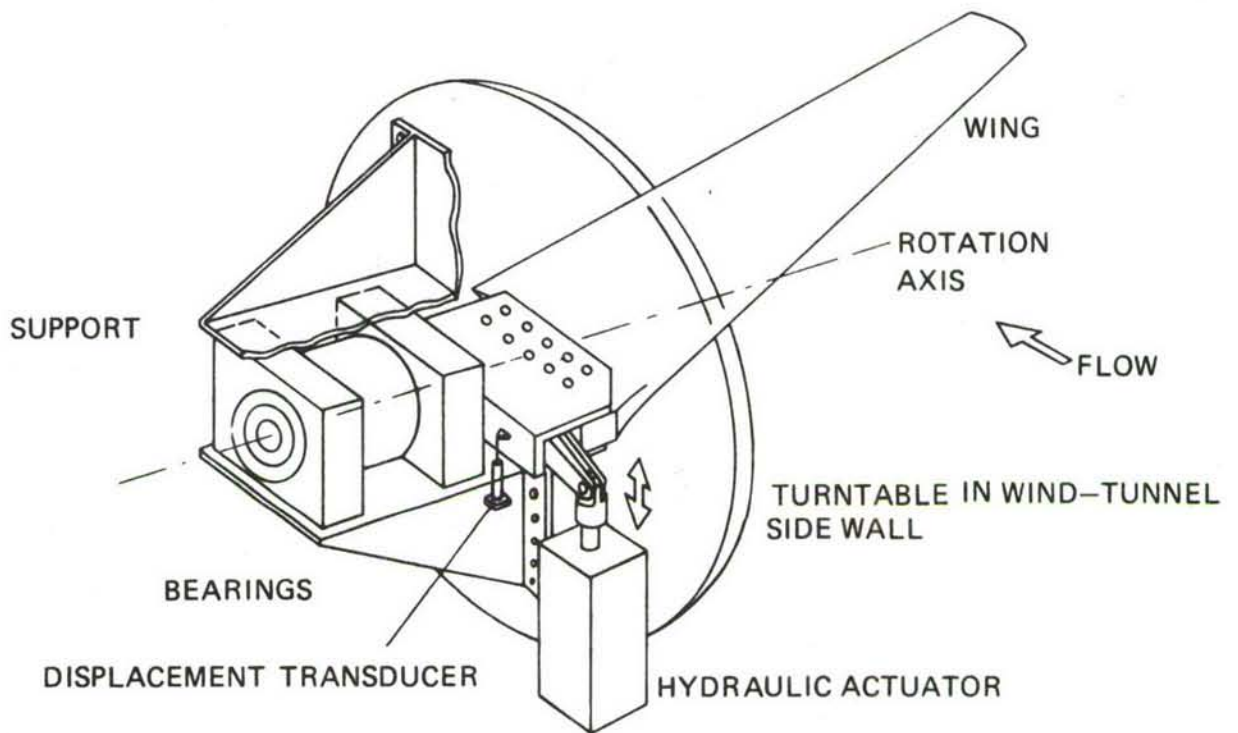


Fig. 1 Schematic view of test set-up

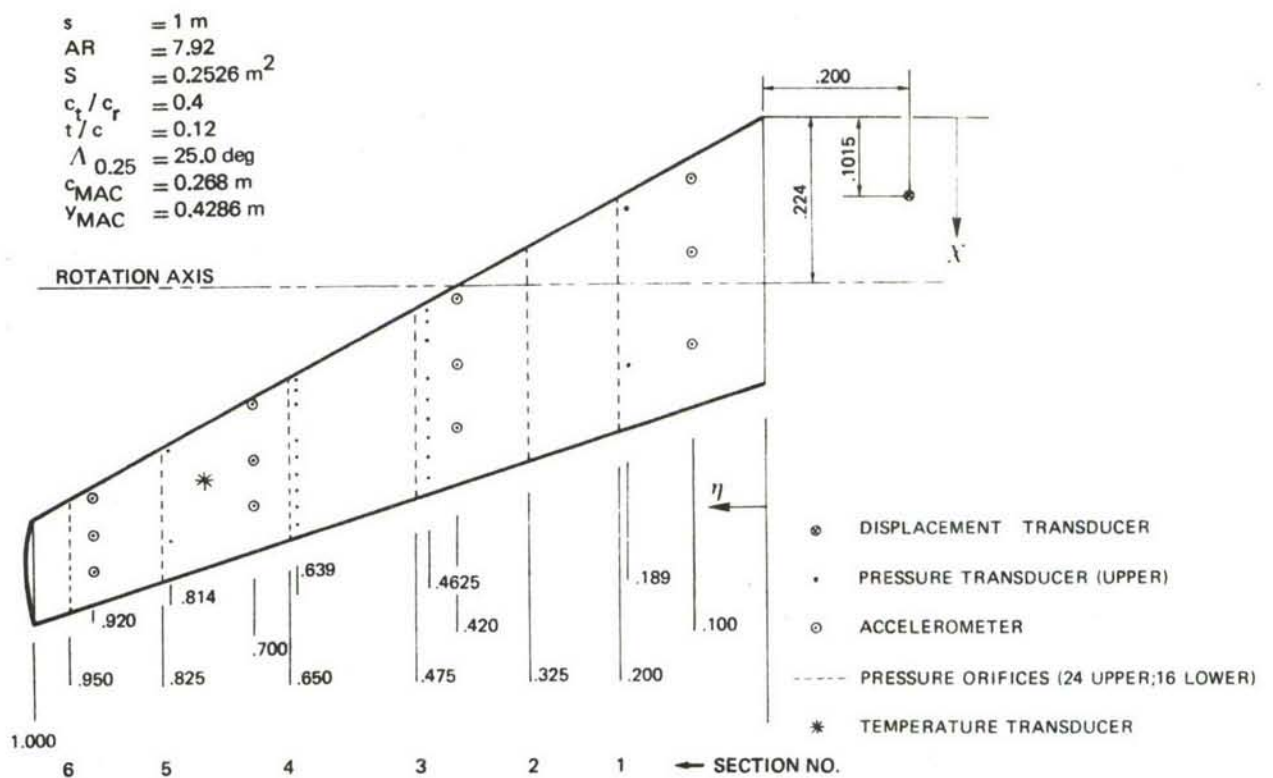


Fig. 2 Wing planform and measuring points

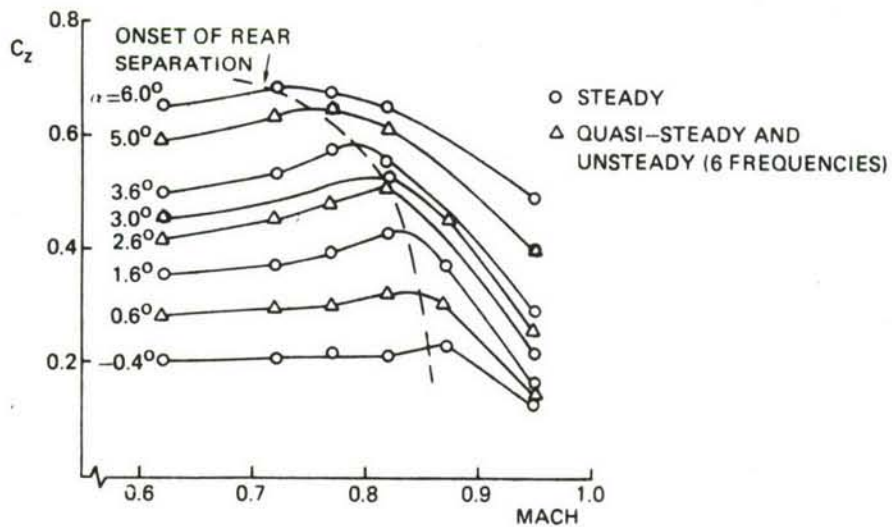


Fig. 3 Test conditions for LANN model

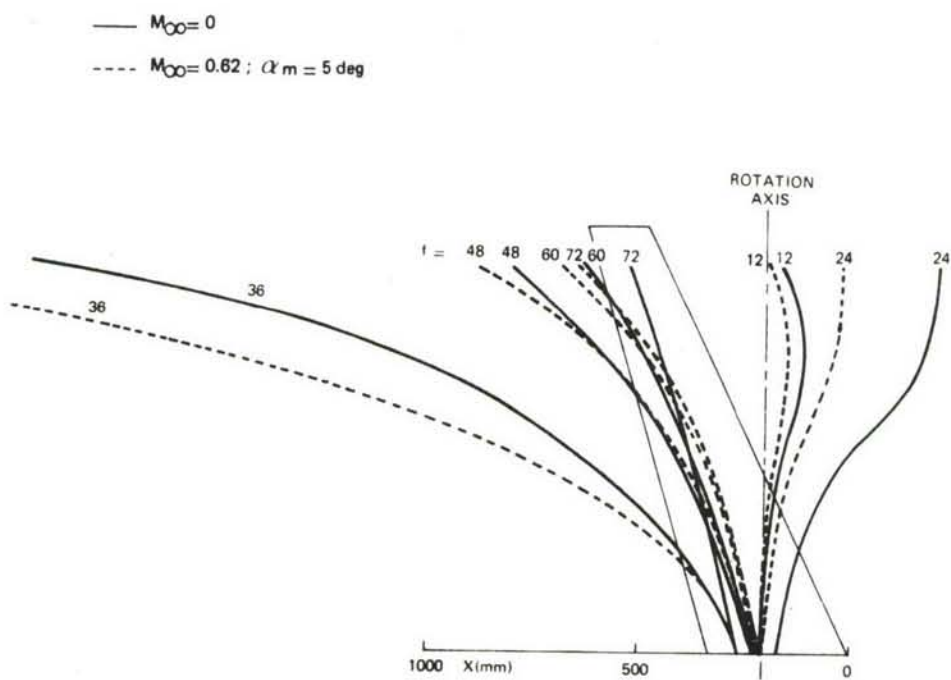


Fig. 4 Influence of Mach number and frequency on node line position

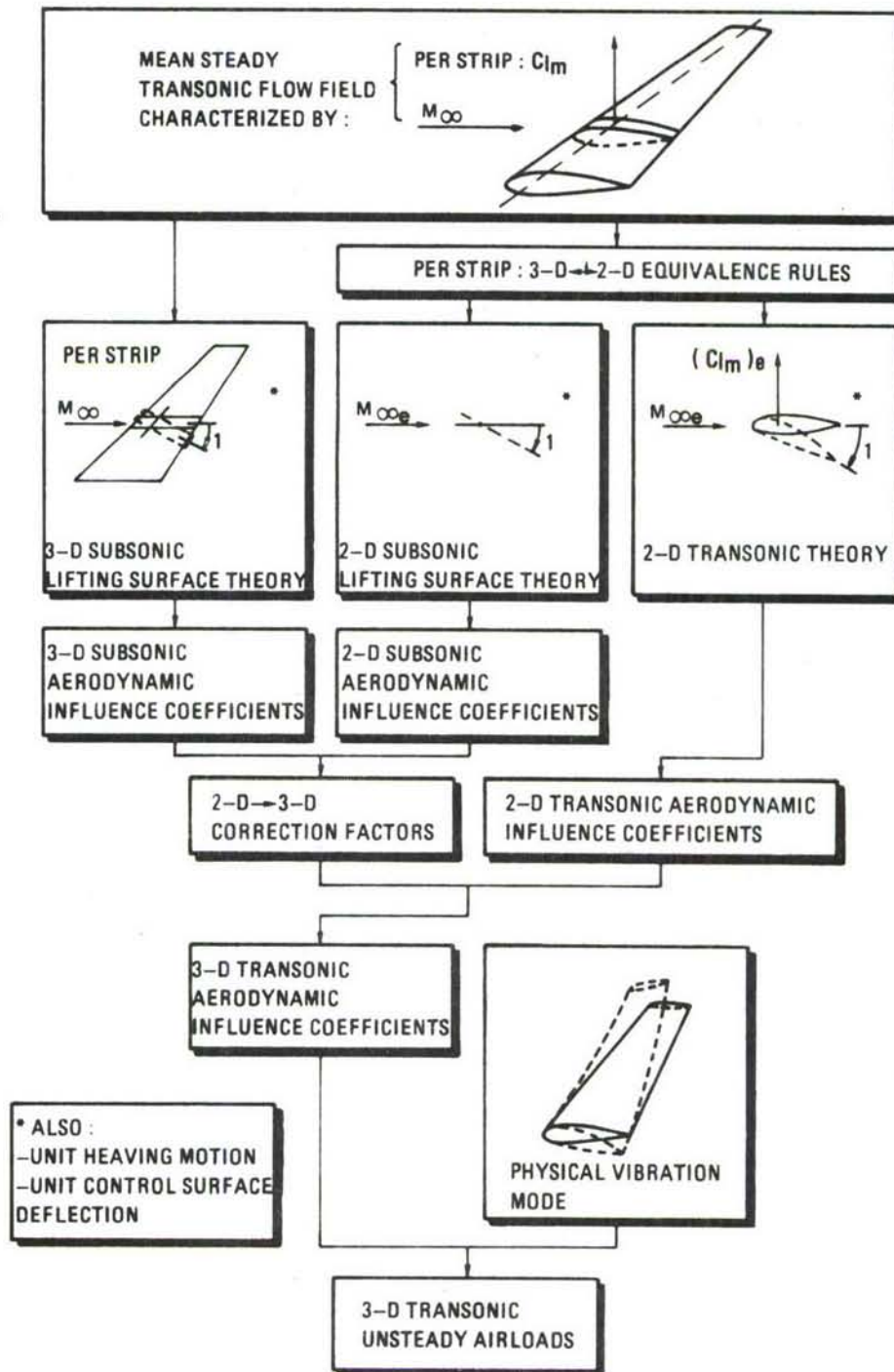


Fig. 5 Outline of quasi-3-d method

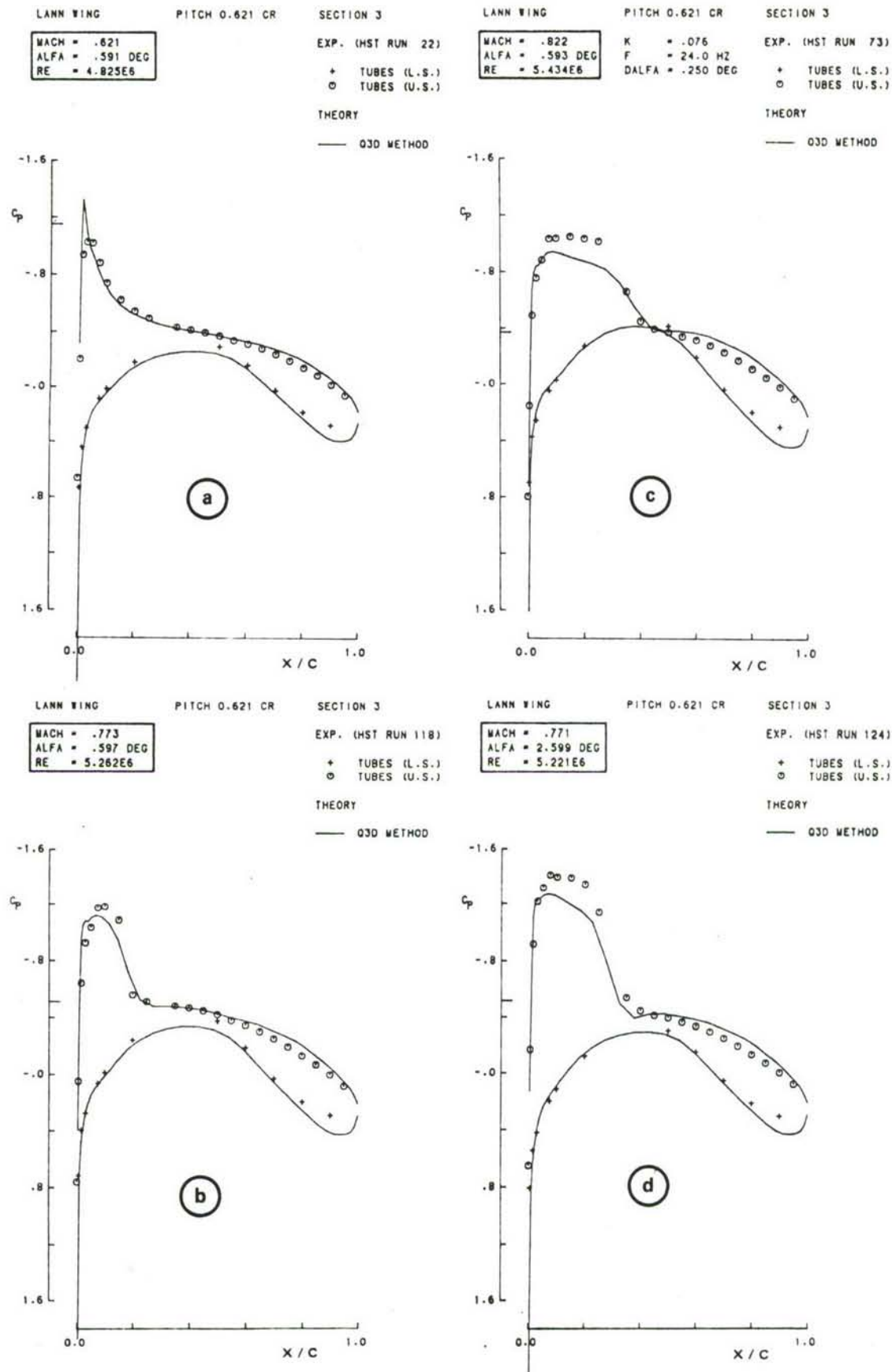


Fig. 6 Mean steady pressure distributions on section 3

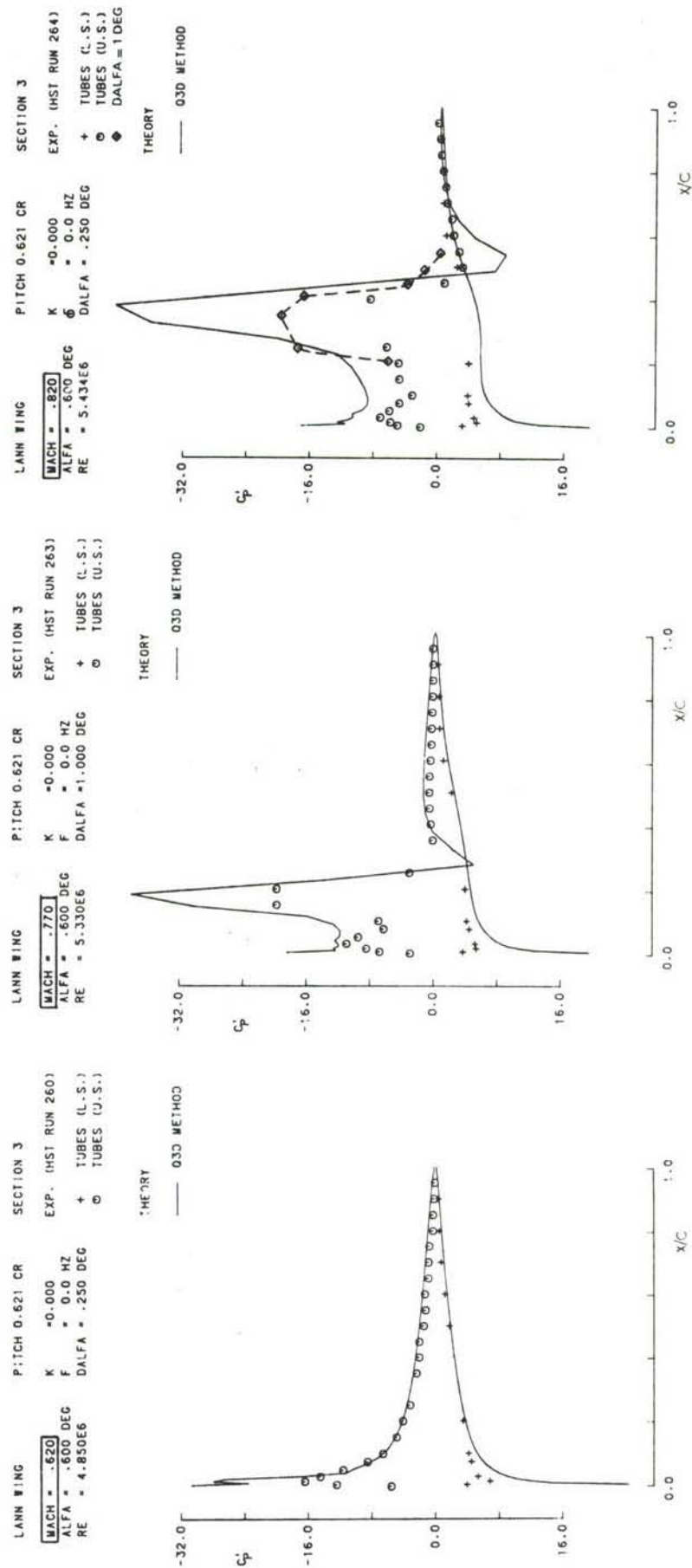


Fig. 7 Quasi-steady pressure distributions on section 3 ($\alpha_o = 0.6$ deg)

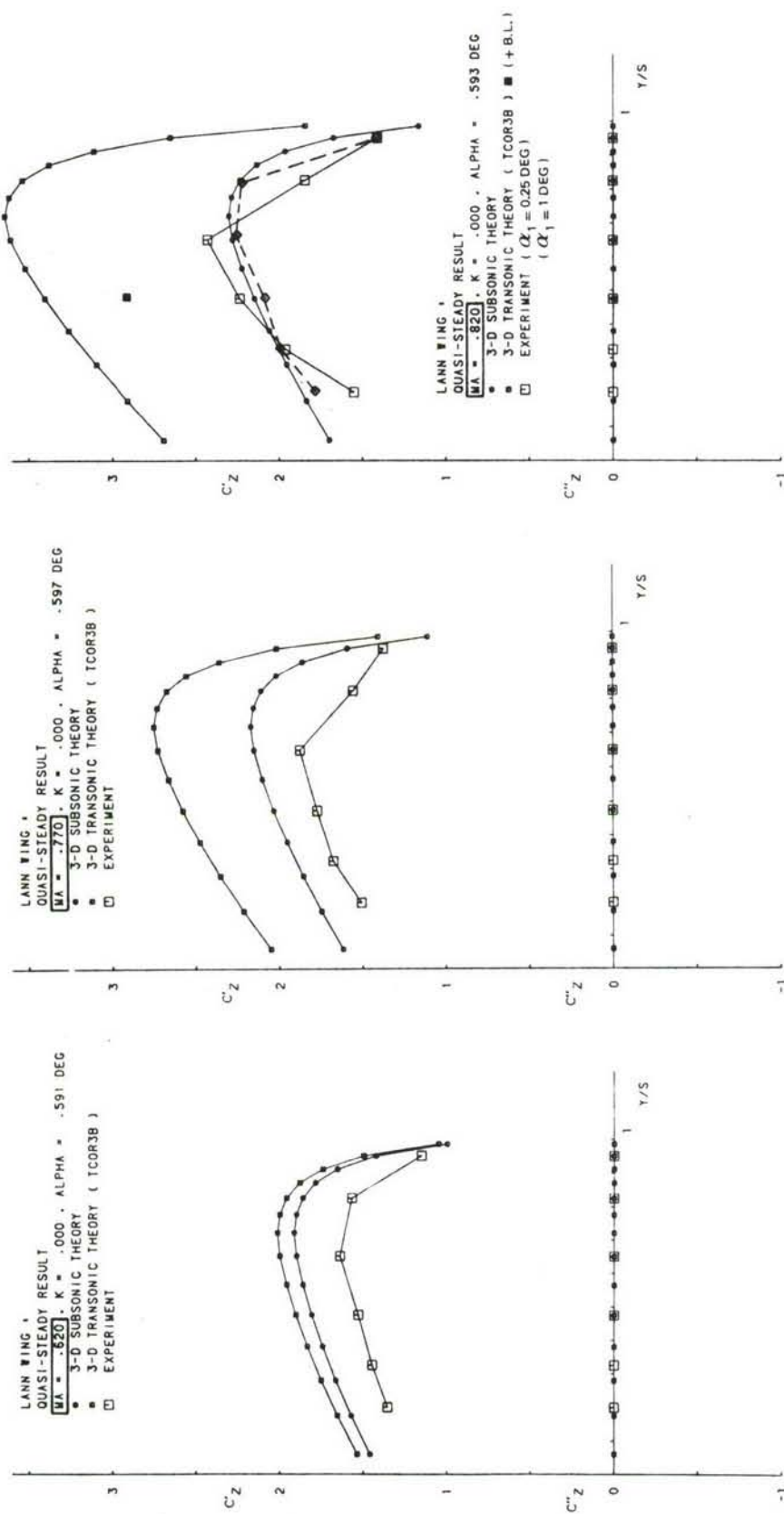


Fig. 8 Quasi-steady sectional lift coefficient ($\alpha_0 = 0.6$ deg)

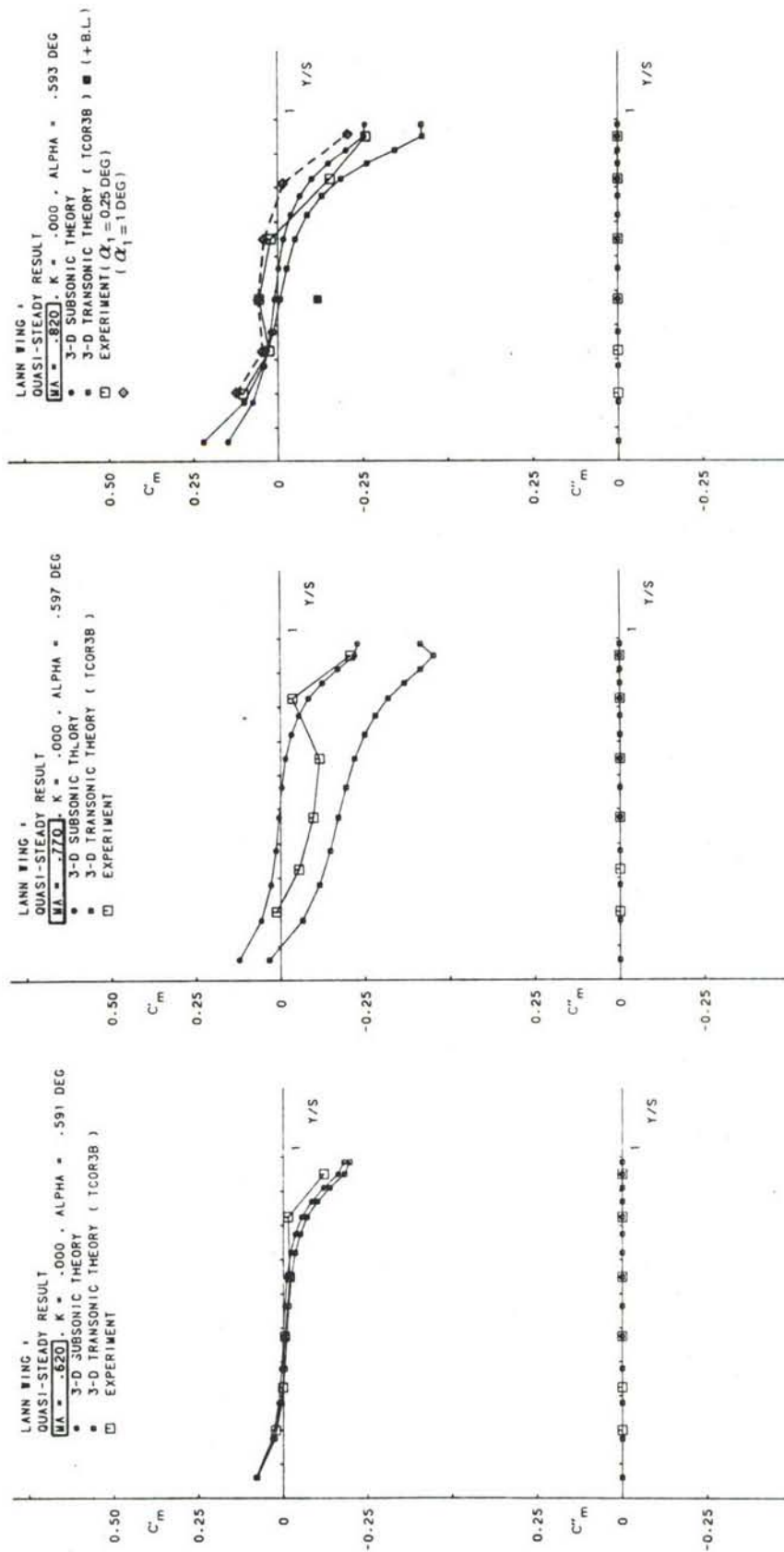


Fig. 9 Quasi-steady sectional moment coefficients ($\alpha_0 = 0.6 \text{ deg}$)

LANN WING OSCILLATING IN PITCH

$\alpha_m = 0.6 \text{ DEG}$
 $\alpha_1 = 0.25 \text{ DEG}$
 $f = 0. \text{Hz}$
 $k = 0$

EXPERIMENT

- + $\alpha_1 = 0.25 \text{ DEG}$
- x $\alpha_1 = 1 \text{ DEG}$
- 3-D SUBS. THEORY
- Q-3-D TRANS. THEORY (INVISCID)

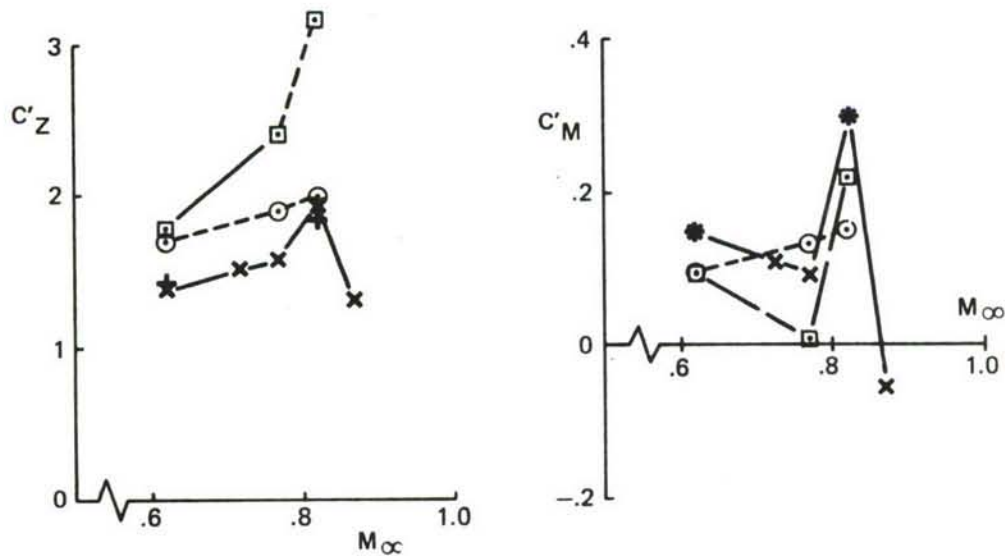


Fig. 10 Quasi-steady wing lift and moment coefficients ($\alpha_m = 0.6 \text{ deg}$)

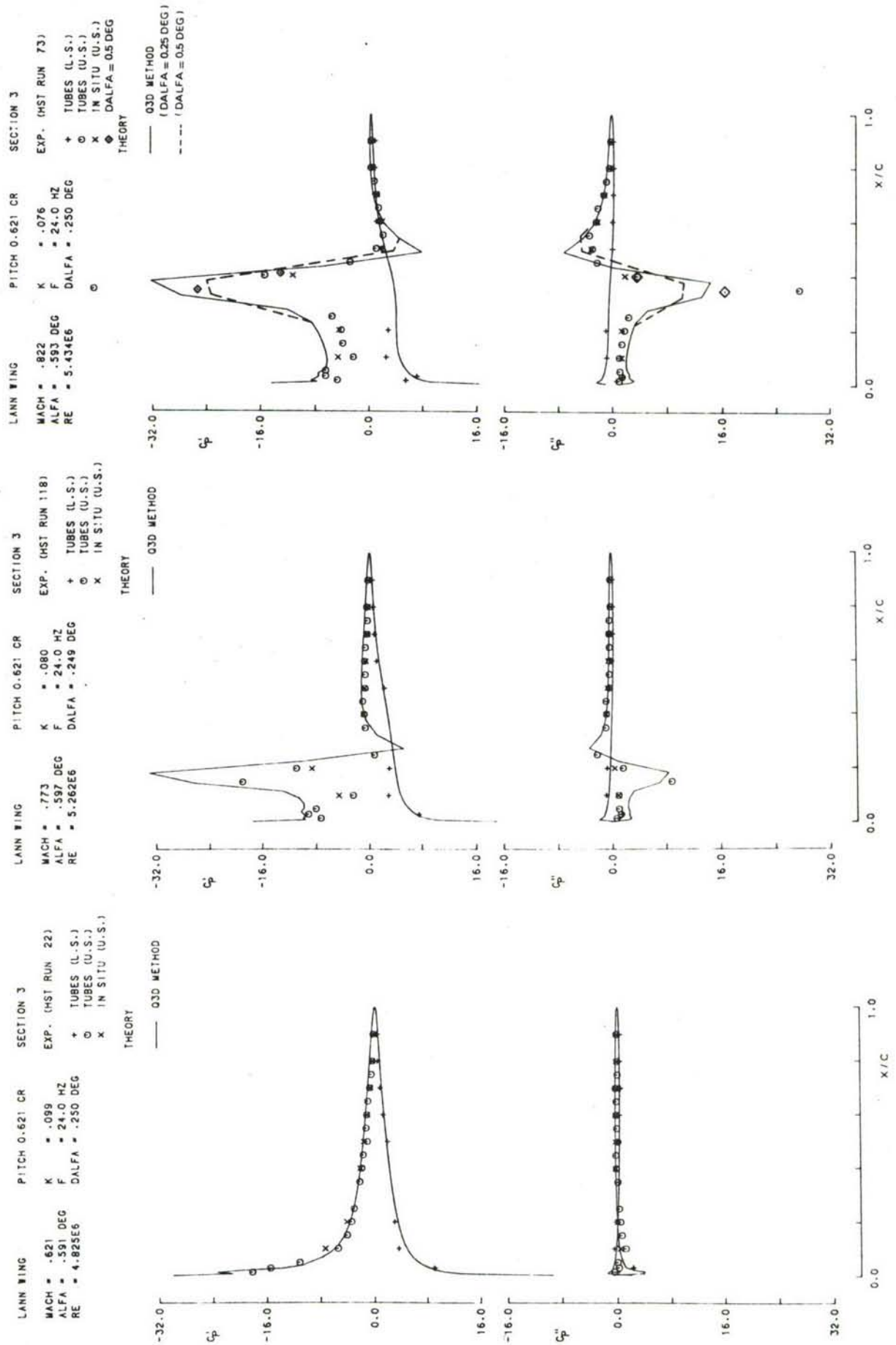


Fig. 11 Unsteady pressure distributions on section 3 ($\alpha_0 = 0.6$ deg, $f = 24$ Hz)

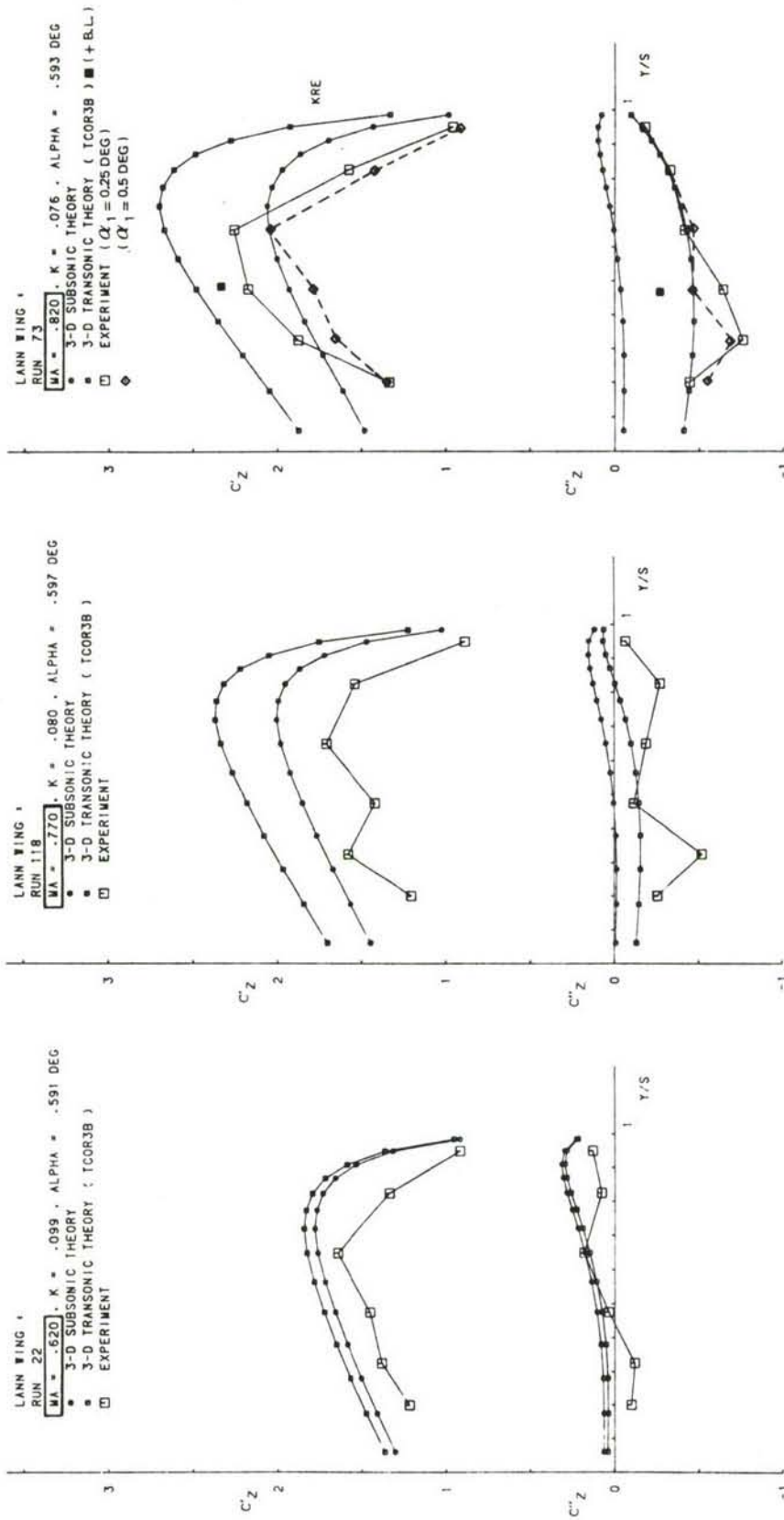


Fig. 12 Unsteady sectional lift coefficients ($\alpha_0 = 0.6$ deg, $f = 24$ Hz)

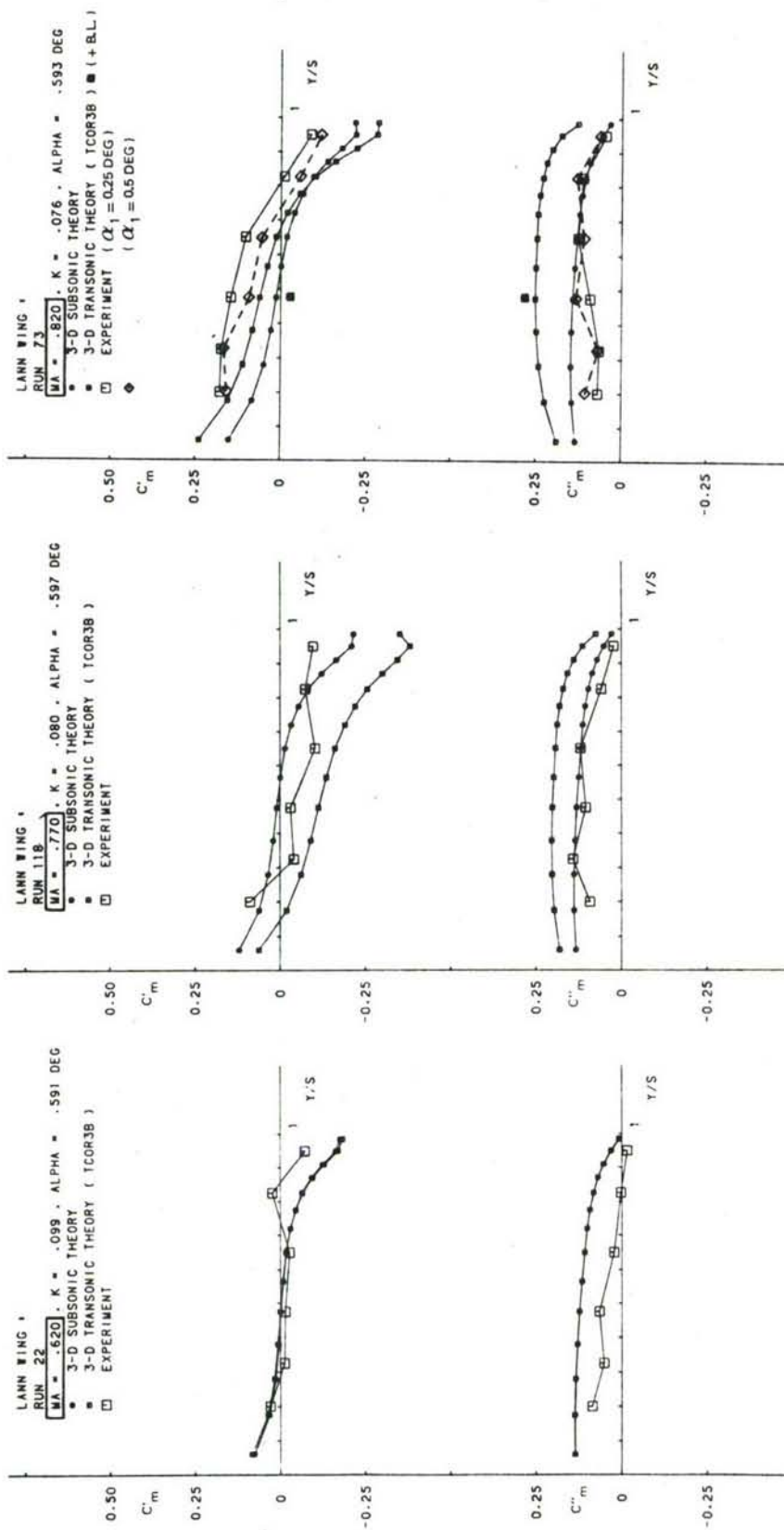


Fig. 13 Unsteady sectional moment coefficients ($\alpha_0 = 0.6$ deg, $f = 24$ Hz)

LANN WING OSCILLATING IN PITCH

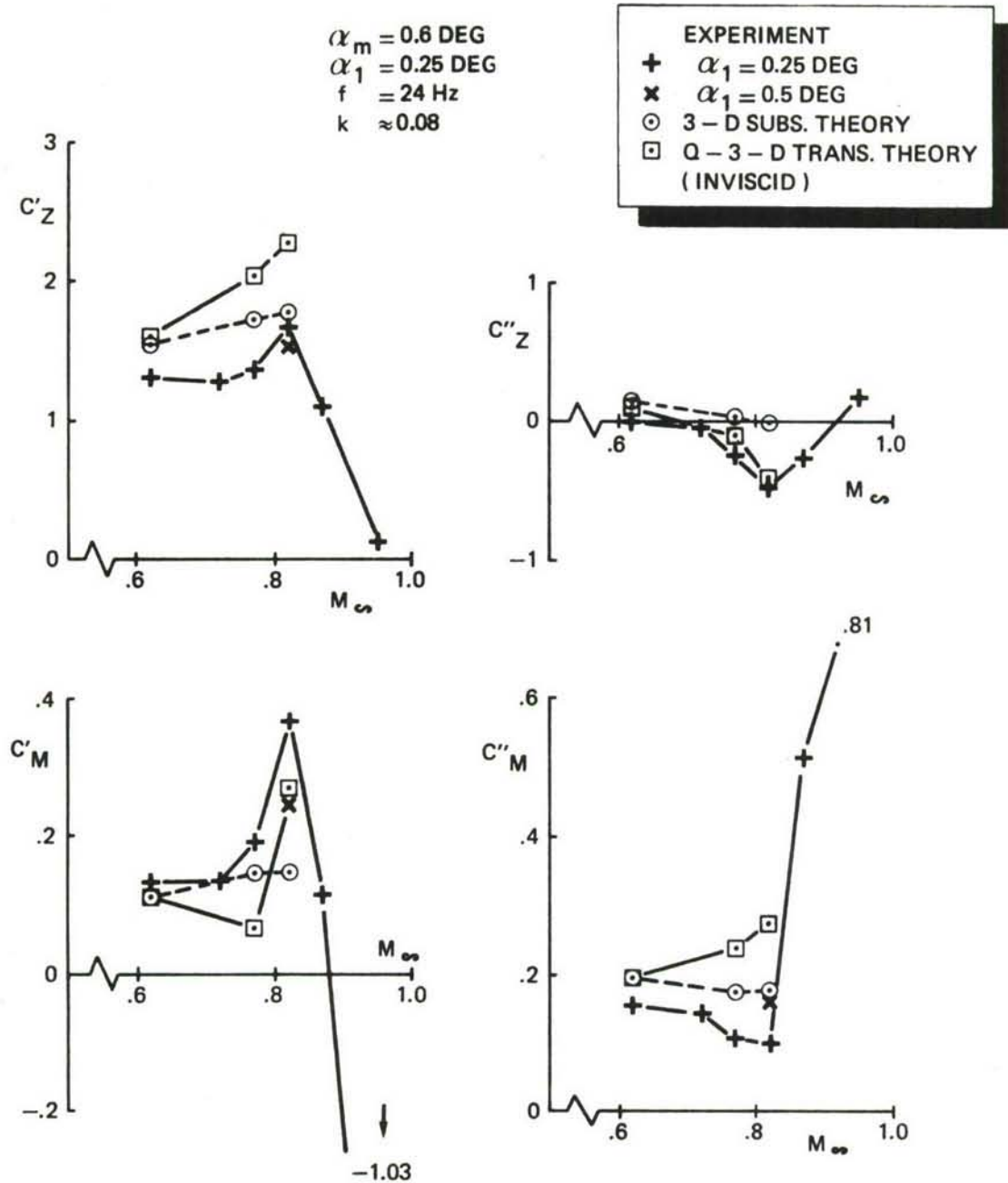


Fig. 14 Unsteady wing lift and moment coefficients ($\alpha_m = 0.6 \text{ deg}$, $f = 24 \text{ Hz}$)

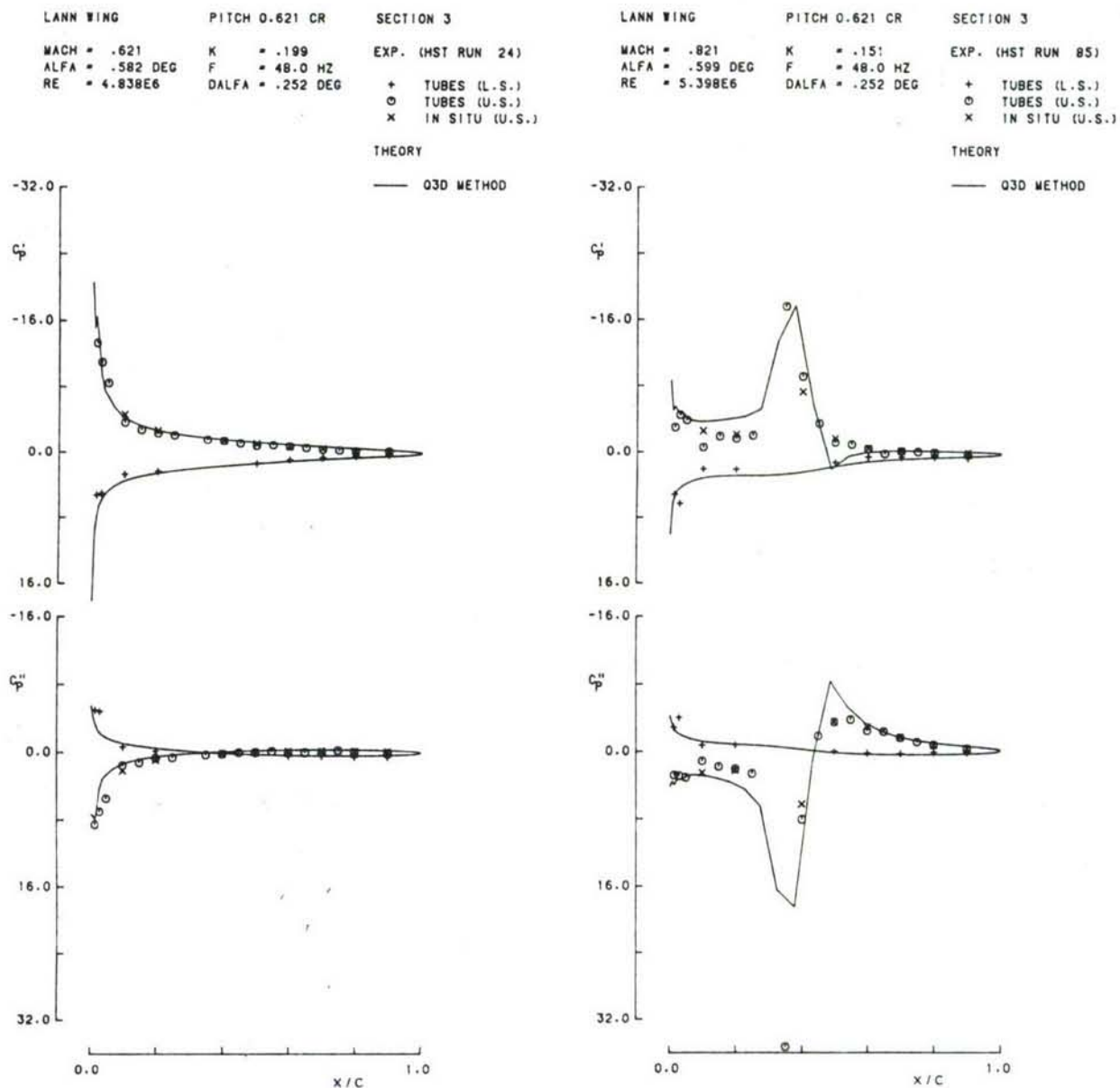
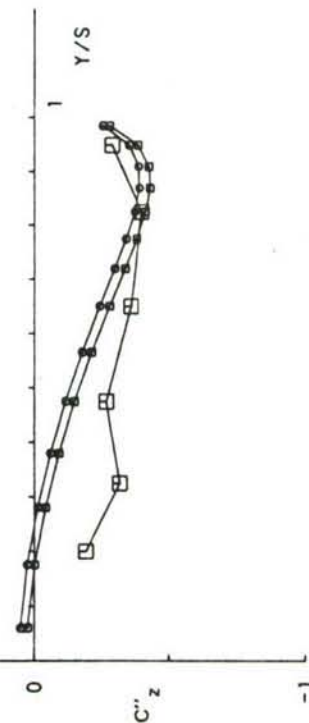
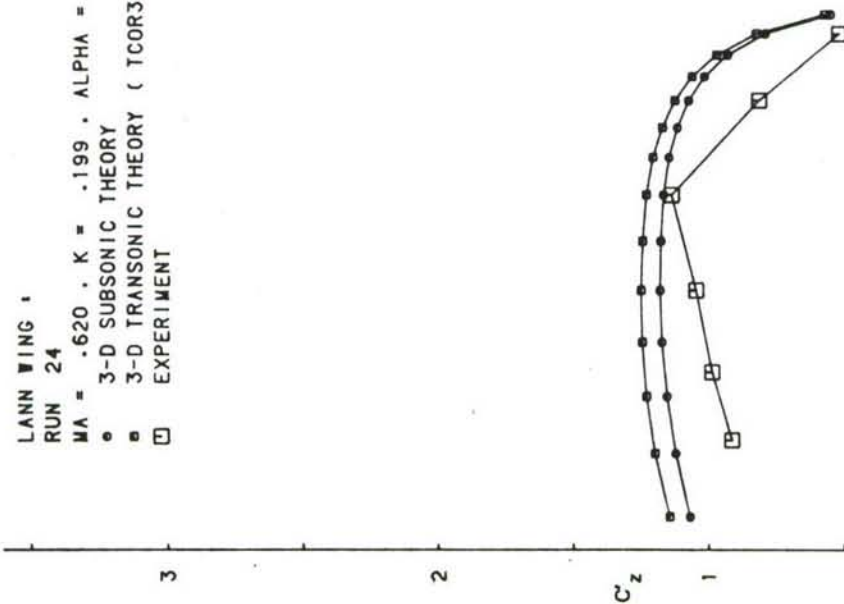


Fig. 15 Unsteady pressure distributions on section 3 ($\alpha_0 = 0.6$ deg, $f = 48$ Hz)

LANN WING :
 RUN 24
 MA = .620 , K = .199 , ALPHA = .582 DEG
 • 3-D SUBSONIC THEORY
 • 3-D TRANSONIC THEORY (TCOR3B)
 □ EXPERIMENT



LANN WING :
 RUN 85
 MA = .820 , K = .151 , ALPHA = .599 DEG
 • 3-D SUBSONIC THEORY
 • 3-D TRANSONIC THEORY (TCOR3B)
 □ EXPERIMENT

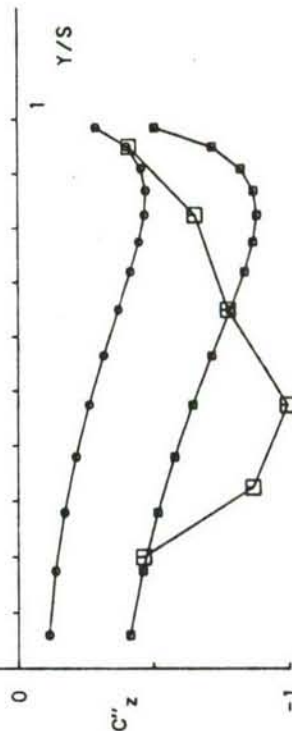
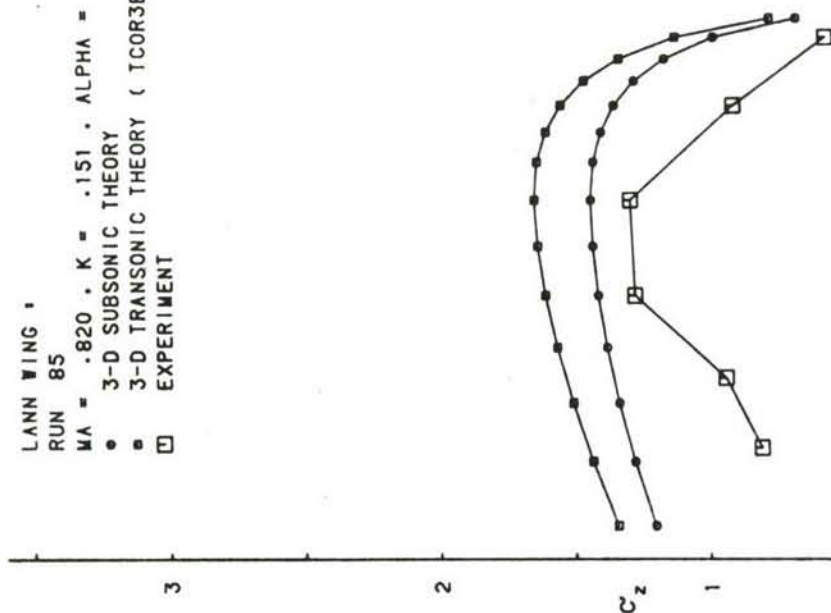


Fig. 16 Unsteady sectional lift coefficients ($\alpha_0 = 0.6$ deg, $f = 48$ Hz)

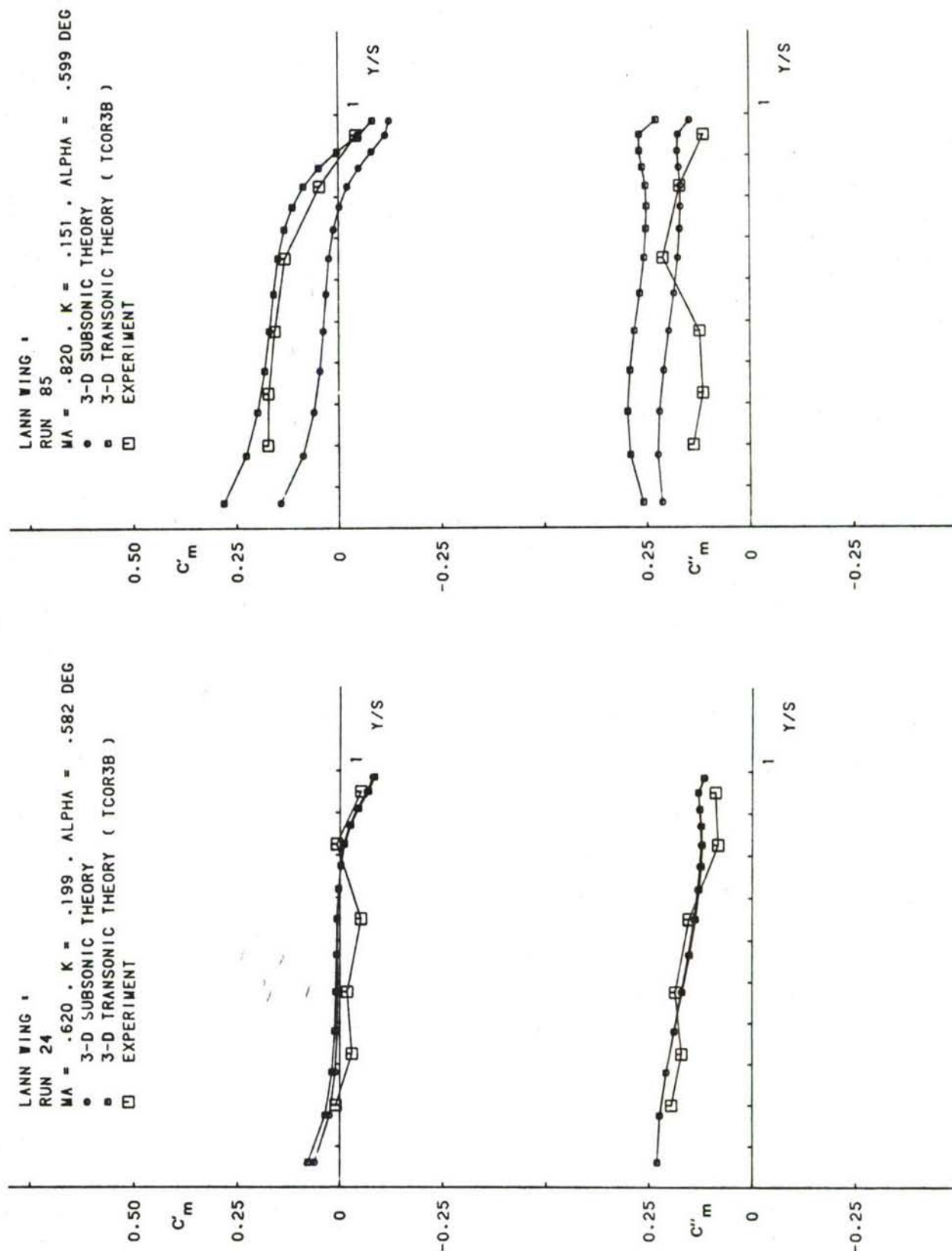


Fig. 17 Unsteady sectional moment coefficients ($\alpha_0 = 0.6$ deg, $f = 48$ Hz)

LANN WING OSCILLATING IN PITCH

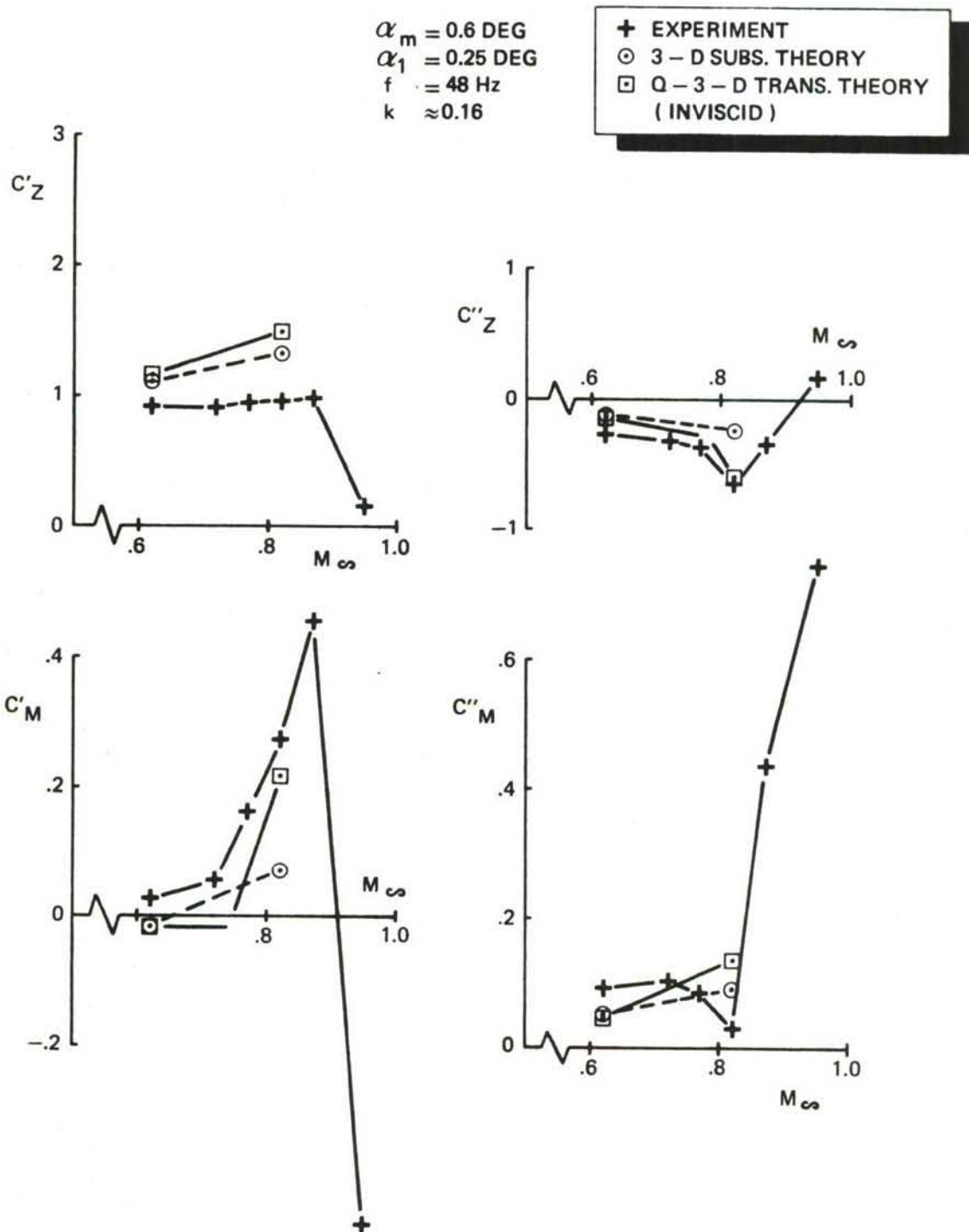


Fig. 18 Unsteady wing lift and moment coefficients ($\alpha_m = 0.6 \text{ deg}$, $f = 48 \text{ Hz}$)

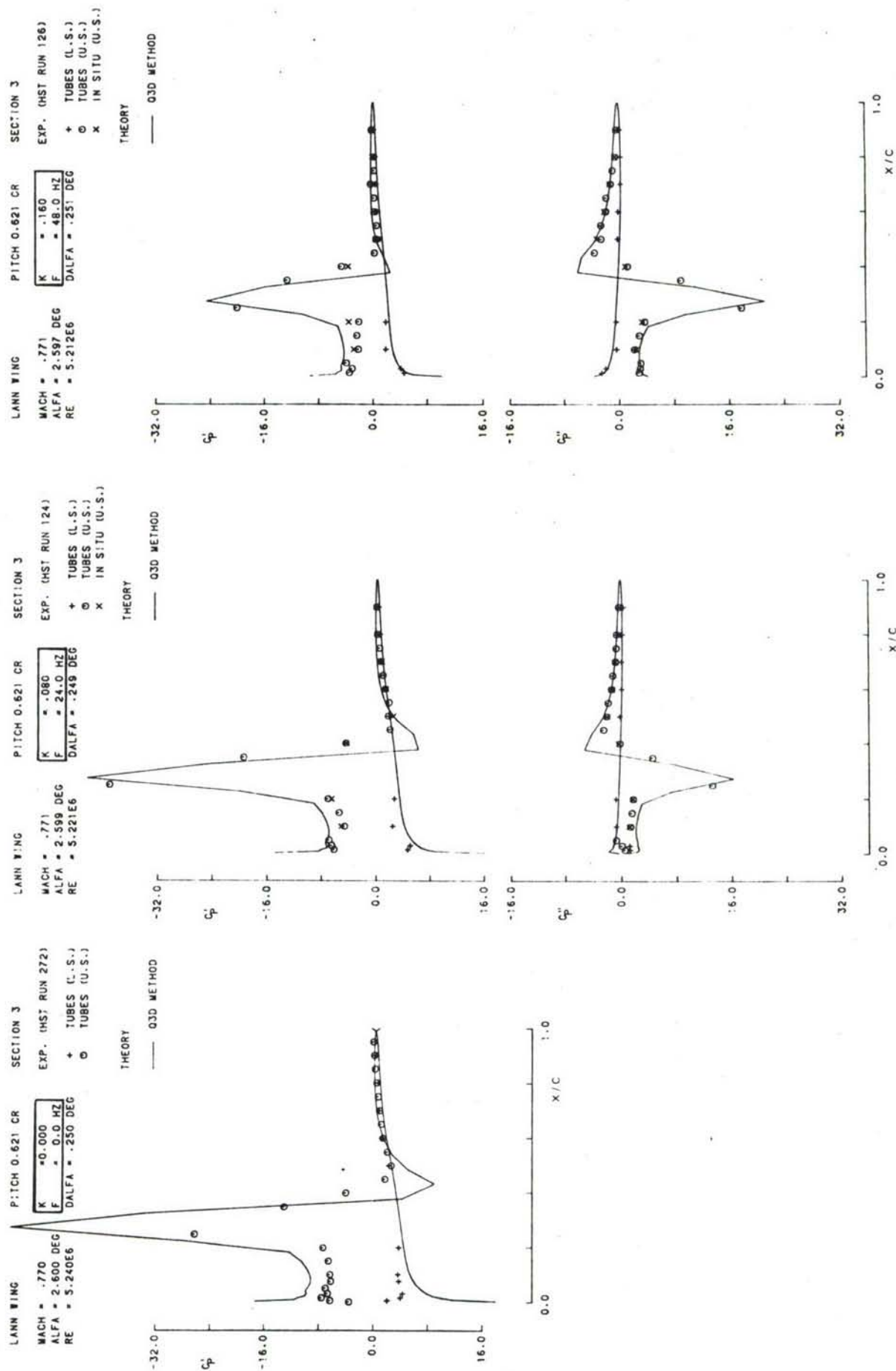


Fig. 19 Quasi-steady and unsteady pressure distributions on section 3 ($\alpha_0 = 2.6$ deg, $M_\infty = 0.77$)

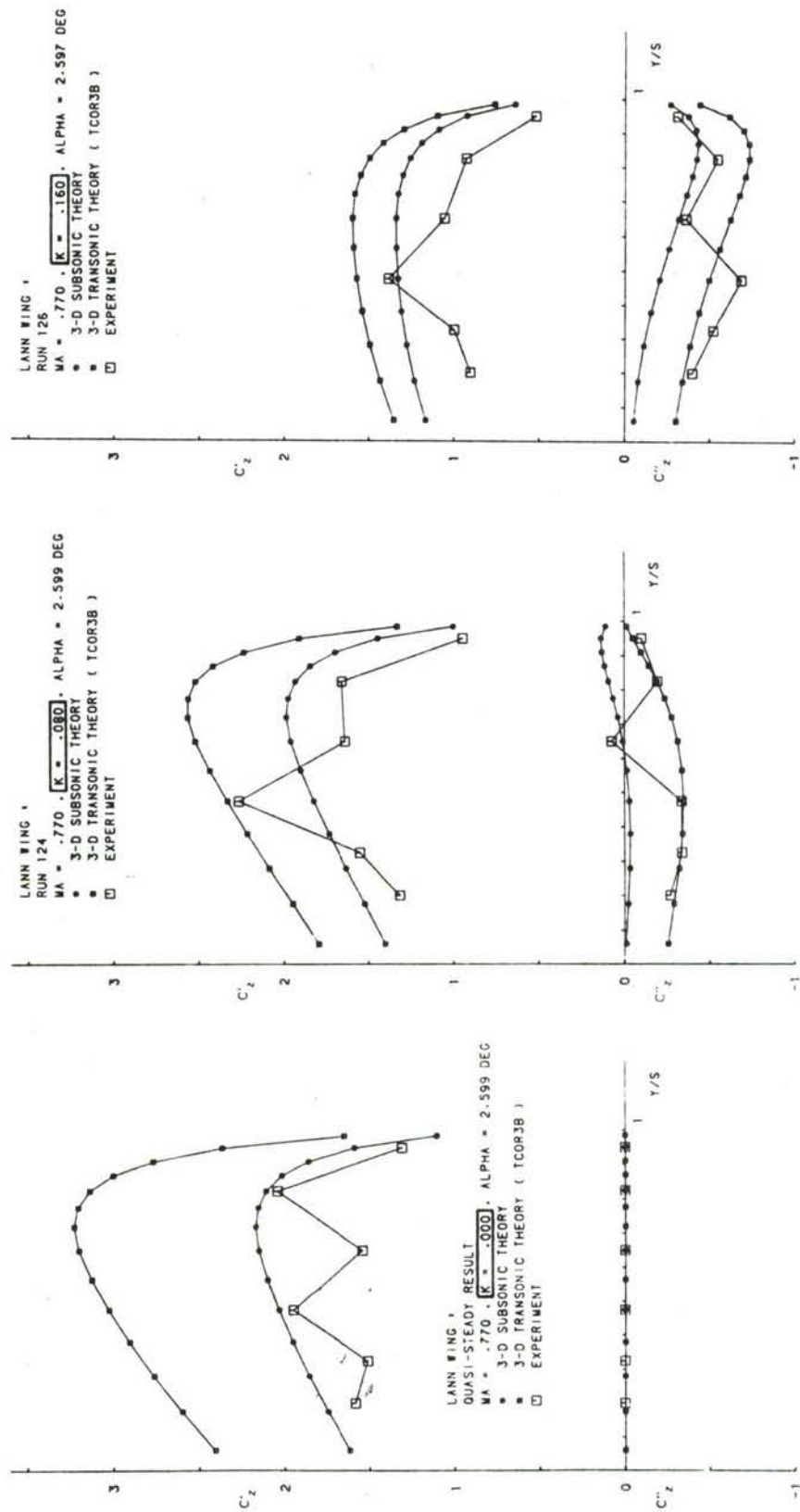


Fig. 20 Unsteady sectional lift coefficients ($\alpha_0 = 2.6$ deg, $M_\infty = 0.77$)

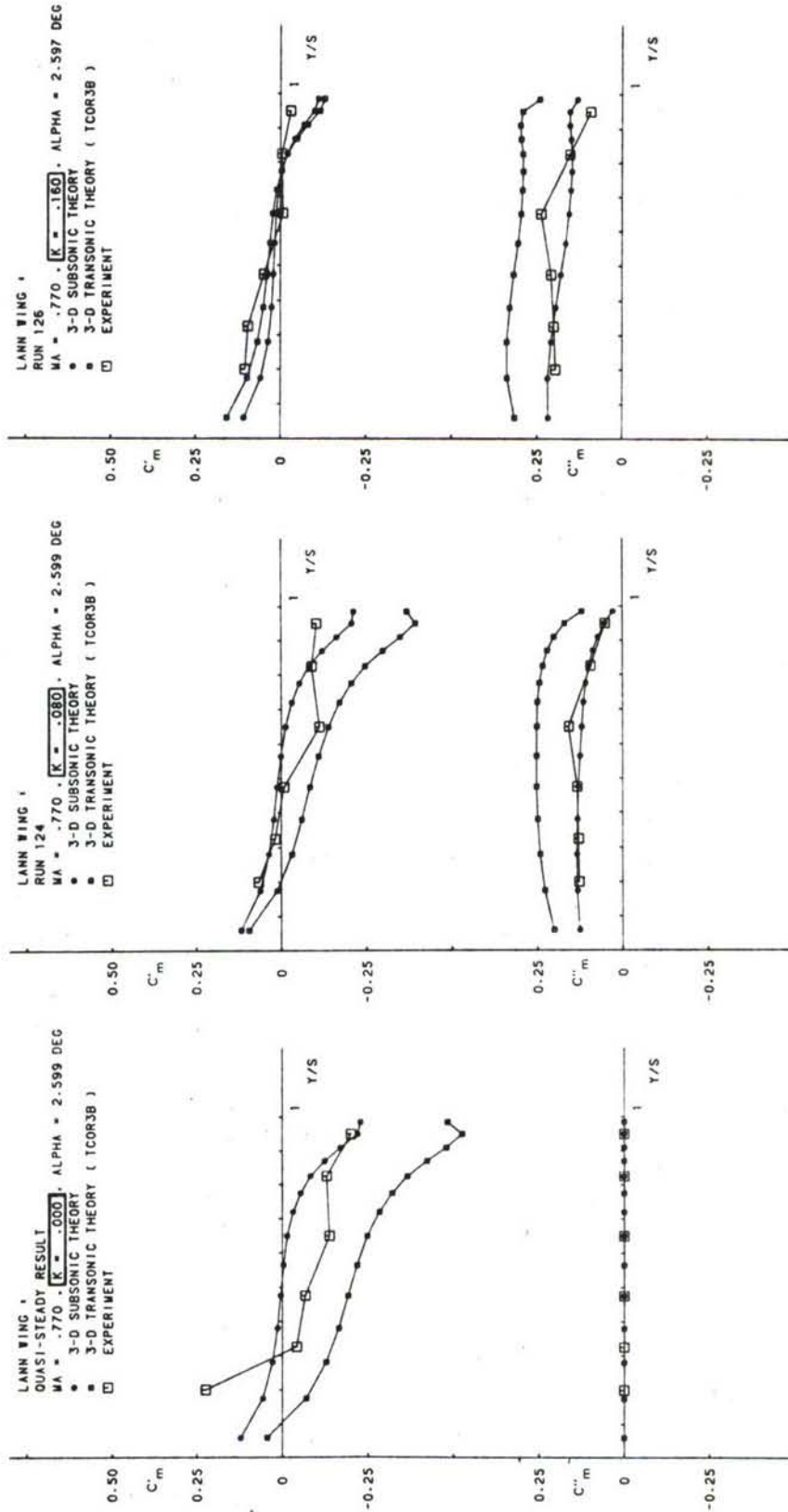


Fig. 21 Unsteady sectional moment coefficients ($\alpha_0 = 2.6^\circ$, $M_\infty = 0.77$)

LANN WING OSCILLATING IN PITCH

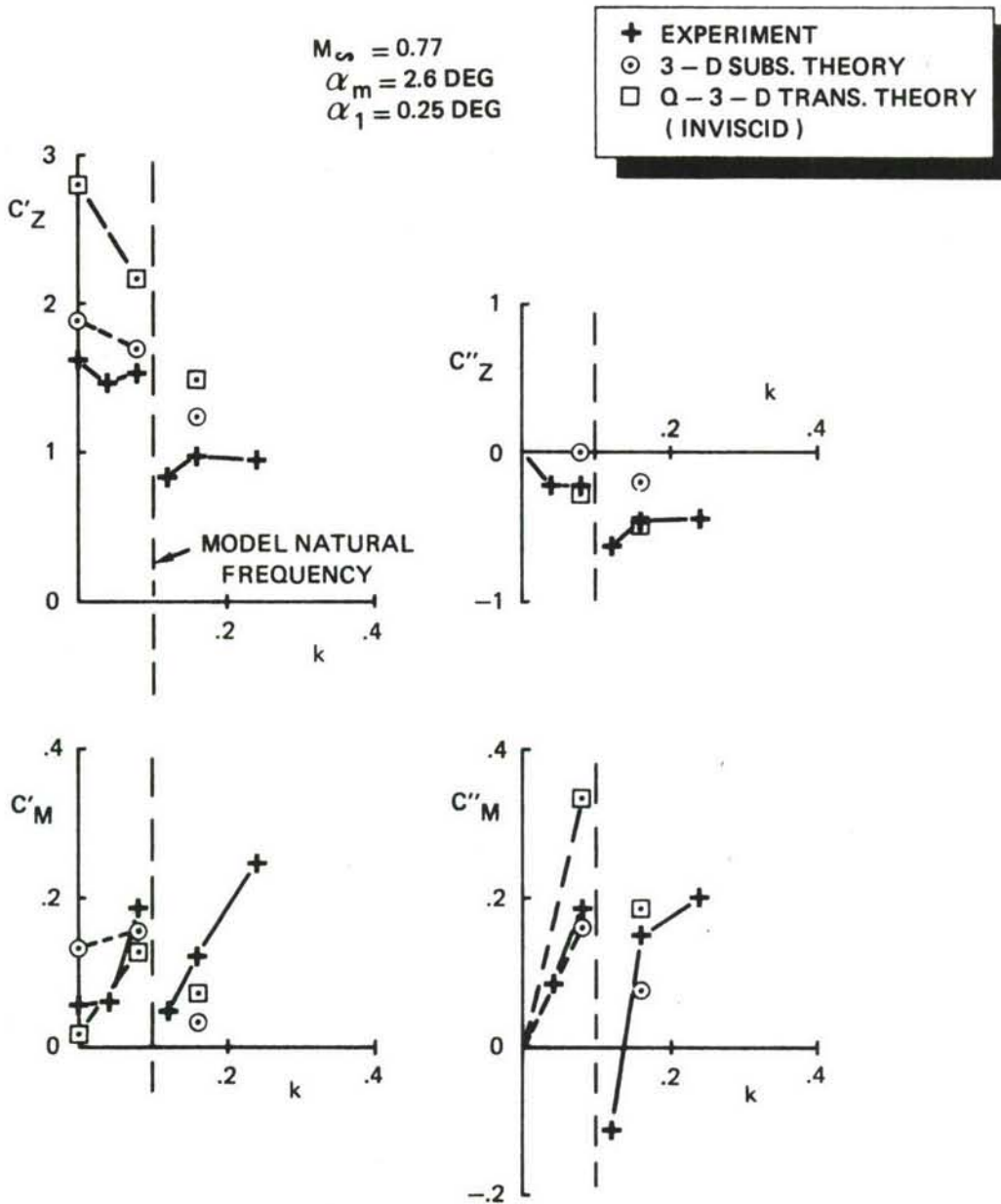


Fig. 22 Unsteady wing lift and moment coefficients ($\alpha_m = 2.6 \text{ deg}$, $M_\infty = 0.77$)

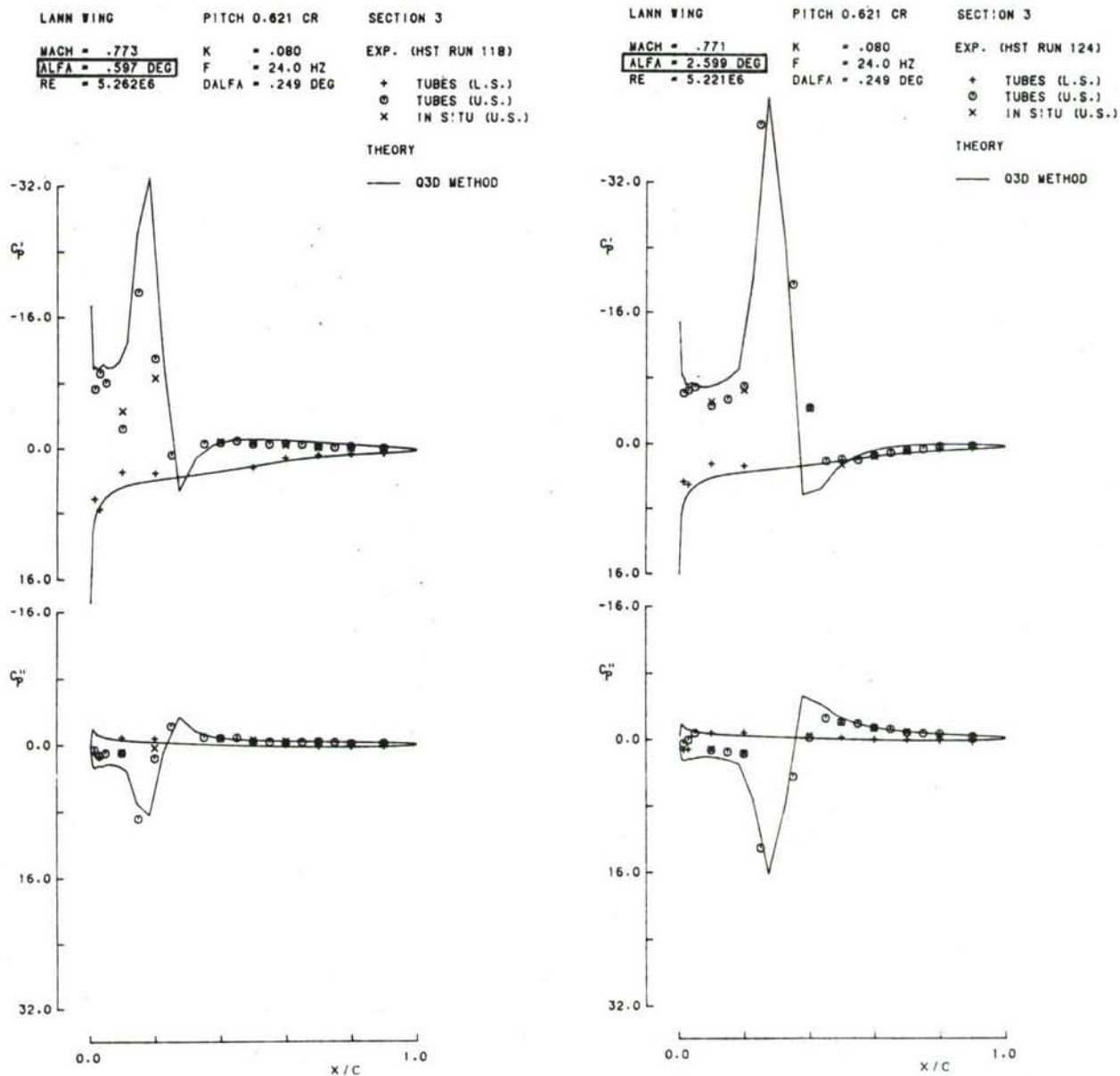


Fig. 23 Unsteady pressure distributions on section 3 ($M_\infty = 0.77$, $f = 24$ Hz)

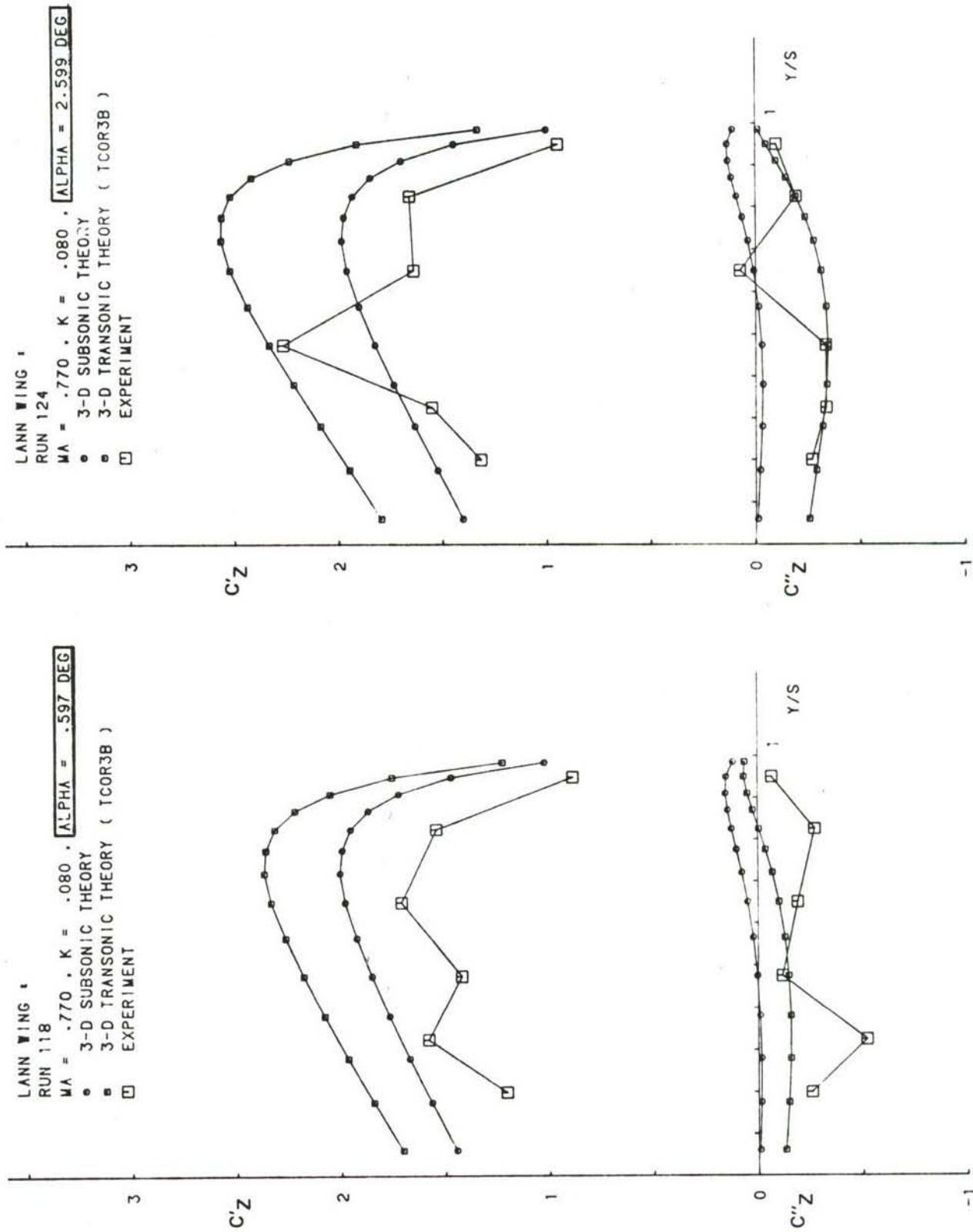


Fig. 24 Unsteady sectional lift coefficients ($M_\infty = 0.77$, $f = 24$ Hz)

LANN WING OSCILLATING IN PITCH

$M_\infty = 0.77$
 $\alpha_1 = 0.25 \text{ DEG}$
 $f = 24 \text{ Hz}$
 $k = 0.08$

\oplus EXPERIMENT
 \odot 3 - D SUBS. THEORY
 \square Q - 3 - D TRANS. THEORY (INVISCID)

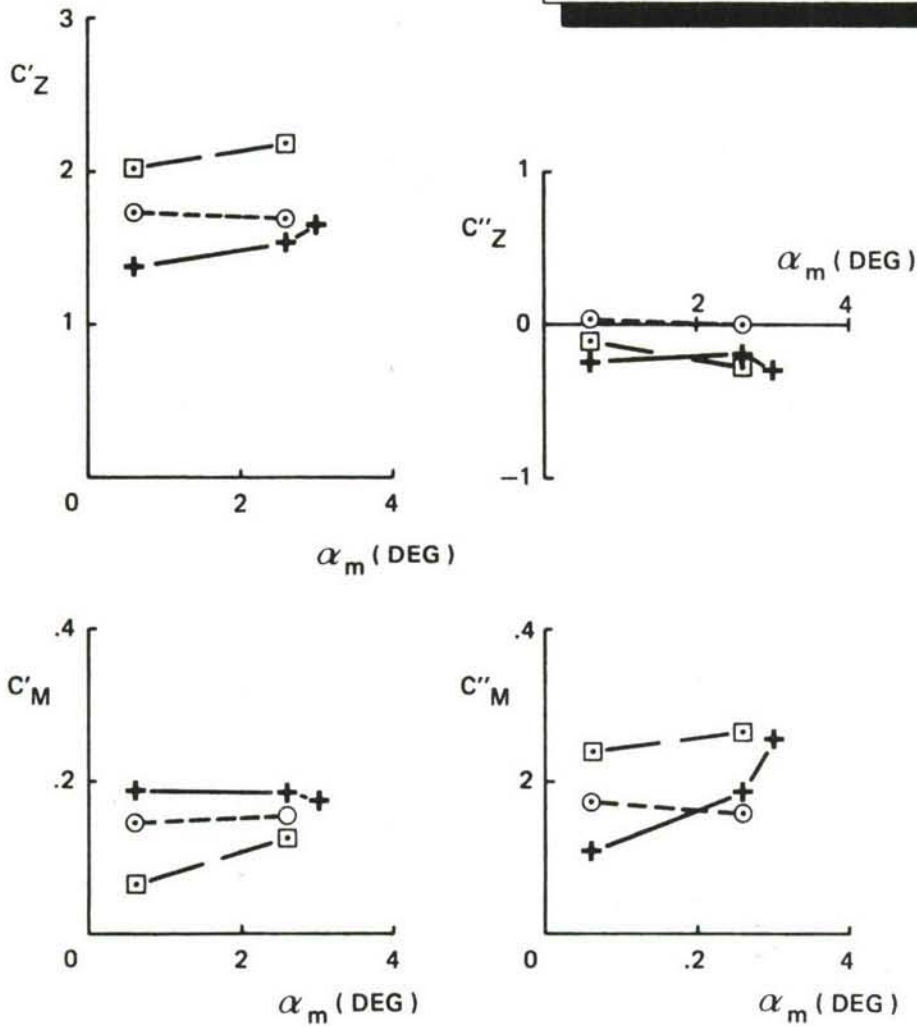


Fig. 26 Unsteady wing lift and moment coefficients ($M_\infty = 0.77$, $f = 24 \text{ Hz}$)

- 1 Horsten, J.J.,
den Boer, R.G.,
Zwaan, R.J.
Unsteady transonic pressure measurements
on a semi-span wind-tunnel model of a
transport-type supercritical wing.
(LANN model).
NLR TR 82069 U Parts I and II, July 1982
- 2 Hinson, B.L.
Burdges, K.P.
Acquisition and application of transonic
wing and far-field test data for three-
dimensional computational method evaluation.
Report AFOSR-TR-80-0421, 1980.
- 3 Houwink, R.,
van der Vooren, J.
Improved version of LTRAN2 for unsteady
transonic flow computations.
AIAA Journal, Vol. 18, No. 8, pp. 1008-1010,
August 1980.
- 4 Steiginga, A.,
Meijer, J.J.
A revised-quasi-3 dimensional concept to
determine unsteady airloads on oscillating
high-aspect ratio wings in transonic flow.
NLR TR 82062 L, June 1982.
- 5 Houwink, R.,
Kraan, A.N.,
Zwaan, R.J.
Wind-tunnel study of the flutter character-
istics of a supercritical wing.
Journal of Aircraft, Vol. 19, No. 5,
pp. 400-405, May 1982.
- 6 Houwink, R.
Results of a new version of the LTRAN2-NLR
code (LTRANV) for unsteady viscous tran-
sonic flow computations.
NLR TR 81078 U, 1981.